

# Plasma motions and compressive wave energetics in the solar corona and solar wind from radio wave scattering observations

FRANCESCO AZZOLLINI,<sup>1</sup> A. GORDON EMSLIE,<sup>2</sup> DANIEL L. CLARKSON,<sup>1</sup> NICOLINA CHRYSAPHI,<sup>3,1</sup> AND  
EDUARD P. KONTAR<sup>1</sup>

<sup>1</sup>*School of Physics & Astronomy, University of Glasgow, Glasgow, G12 8QQ, UK*

<sup>2</sup>*Department of Physics & Astronomy, Western Kentucky University, Bowling Green, KY 42101, USA*

<sup>3</sup>*Sorbonne Université, École Polytechnique, Institut Polytechnique de Paris, CNRS, Laboratoire de Physique des Plasmas (LPP), 75005 Paris, France*

## ABSTRACT

Radio signals propagating via the solar corona and solar wind are significantly affected by compressive waves, impacting properties of solar bursts as well as sources viewed through the turbulent solar atmosphere. While static fluctuations scatter radio waves elastically, moving, turbulent or oscillating density irregularities act to broaden the frequency of the scattered waves. Using a new anisotropic density fluctuation model from the kinetic scattering theory for solar radio bursts, we deduce the plasma velocities required to explain observations of spacecraft signal frequency broadening. The inferred velocities are consistent with motions that are dominated by the solar wind at distances  $\gtrsim 10 R_{\odot}$ , but the levels of frequency broadening for  $\lesssim 10 R_{\odot}$  require additional radial speeds  $\sim (100\text{--}300) \text{ km s}^{-1}$  and/or transverse speeds  $\sim (20\text{--}70) \text{ km s}^{-1}$ . The inferred radial velocities also appear consistent with the sound or proton thermal speeds, while the speeds perpendicular to the radial direction are consistent with non-thermal motions measured via coronal Doppler-line broadening, interpreted as Alfvénic fluctuations. Landau damping of parallel propagating ion-sound (slow MHD) waves allow an estimate of the proton heating rate. The energy deposition rates due to ion-sound wave damping peak at a heliocentric distance of  $\sim (1 - 3) R_{\odot}$  are comparable to the rates available from a turbulent cascade of Alfvénic waves at large scales, suggesting a coherent picture of energy transfer, via the cascade or/and parametric decay of Alfvén waves to the small scales where heating takes place.

**Keywords:** interplanetary scintillation (828), interplanetary turbulence (830), radio bursts (1339), solar corona (1483), solar wind (1534)

## 1. INTRODUCTION

Radio waves propagating in the solar atmosphere are scattered by density fluctuations, affecting the observed properties of radio emission originating either in the solar corona itself or in distant sources close to the location of the Sun in the sky. Solar burst source angular sizes and time profiles are broadened by the density fluctuations, and the apparent source positions are shifted, usually away from the Sun. Typically, extrasolar sources are observed at frequencies  $\omega$  that are signifi-

cantly higher than the plasma frequency  $\omega_{pe}$  of the solar medium through which their emitted radiation propagates and scatters. This results in a scattering mean free path that is much larger than the distance traveled by the radio waves in the turbulent medium. Consequently, such sources experience much weaker scattering than solar radio burst emission at frequencies inherently close to the local plasma frequency (or its second harmonic). Despite this distinction, the properties of solar and extrasolar sources are affected by the same density turbulence, with recent study showing that the propagation of solar and extrasolar radio emission in both strong and weak scattering regimes can be modeled using the same kinetic approach (Kontar et al. 2023). Since the speeds of density fluctuations are much less than the speed of radio waves, scattering is often treated as elastic, resulting primarily in angular broadening of extra-solar point sources (e.g., Machin & Smith 1952; Hewish 1958; Blesing & Dennison 1972; Anantharamaiah et al. 1994; Ingale et al. 2015), an increase in the angular source sizes of solar radio sources (e.g., Fokker 1965; Steinberg 1972; Riddle 1974; Bastian 1994; Arzner & Magun 1999; Thejappa & MacDowall 2008; Kontar et al. 2017b; Chrysaphi et al. 2018; Krupar et al. 2018; McCauley et al. 2018; Gordovskyy et al. 2019; Kontar et al. 2019; Chrysaphi et al. 2020; Krupar et al. 2020; Murphy et al. 2021; Maguire et al. 2021; Mohan 2021; Musset et al. 2021; Sharma & Oberoi 2021; Clarkson et al. 2021) and changes in the paths of spacecraft signals observed through the turbulent solar atmosphere (e.g., Woo 1978; Razmanov et al. 1980; Bradford & Routledge 1980; Bird 1982; Woo & Goldstein 1994; Efimov et al. 2013; Yakovlev & Pisanko 2018; Wexler et al. 2019; Efimov et al. 2020; Chiba et al. 2022). The density fluctuations are also routinely observed near 1 au (e.g., Celnikier et al. 1983; Marsch & Tu 1990; Krupar et al. 2020; Wang et al. 2024).

The collective Compton scattering from electron density fluctuations (e.g., Akhiezer et al. 1958; Dougherty & Farley 1960; Bingham et al. 2003) that are moving or oscillating perpendicular to the direction of wave propagation can, however, lead to an *inelastic* change in the wavenumber and hence frequency broadening (that is normally a small fraction of the observed frequency). Doppler broadening of radio waves from spacecraft has been extensively studied to diagnose expansion of the solar wind (e.g., Woo 1978), and moving density irregularities have also been analyzed via observations of interplanetary scintillations (e.g., Woo & Gazis 1993; Woo 1996; Morabito 2009; Mejia-Ambriz et al. 2015). The spectral width of the radio-wave signal, or the strength of scintillation, is proportional to the speed of the density irregularity weighted by the amplitude of the density fluctuation. Using multiple receivers to observe interplanetary scintillation, Ekers & Little (1971) found a random velocity component of  $v \simeq (100\text{--}200) \text{ km s}^{-1}$  at  $(5\text{--}10) R_{\odot}$  and less than  $50 \text{ km s}^{-1}$  at  $40 R_{\odot}$ . Somewhat lower fractional velocities  $\delta v/v \simeq 0.25$  of the solar wind speed were deduced by Armstrong & Coles (1972). Armstrong et al. (1986) reported a random velocity component at  $< 12 R_{\odot}$  that was comparable to the bulk flow speed. Assuming a density model of the corona and the fractional amplitude of density fluctuations, Wexler et al. (2020) used spacecraft carrier frequency fluctuations to infer the flow velocity profile in the middle corona (West et al. 2023).

Here we use a recently-developed anisotropic density turbulence model (Kontar et al. 2023) to analyze a large observational dataset of Doppler broadening of spacecraft carrier frequencies and thus determine the speeds of density fluctuations in the space between the Sun and 1 au. The spectral broadening is discussed in terms of solar wind flows, compressive waves, and random plasma motions. By matching observations, we determine the characteristic velocities of density fluctuations and we show how the wavevector anisotropy,  $\alpha = q_{\parallel}/q_{\perp}$ , associated with density fluctuations along versus perpendicular to the solar radius vector, affects these results. The average frequency broadening at  $>10 R_{\odot}$  is found,

in line with the previous works, to be determined mostly by the radial solar wind speed, while closer to the Sun ( $<10 R_\odot$ ), both transverse and radial motions could contribute. Due to the wavenumber anisotropy in the density fluctuations, which are typically elongated along the radial direction ( $\alpha < 1$ ), smaller perpendicular velocities are needed to explain a given amount of frequency broadening. For example, if  $\alpha = 0.25$ , either radial speeds  $\simeq 160 \text{ km s}^{-1}$  or transverse speeds  $\simeq 40 \text{ km s}^{-1}$  are consistent with the observed amount of frequency broadening.

In Section 2 we introduce the model used. In Section 3 we consider the effects of inelastic scattering in the presence of motions perpendicular to the line of sight, and we derive the associated diffusion tensor for radio waves in anisotropic turbulent plasma. We also compare the deduced random motions with non-thermal velocities deduced from the emission line broadening of hot ions.

In Sections 4 and 5 we turn our attention to observed values of the frequency broadening  $\Delta f$ . We derive an expression for the fractional frequency broadening  $\Delta f/f$  in terms of the product of the fluid velocity perpendicular to the line of sight and the wavenumber-weighted line-of-sight integral of the density fluctuation amplitude. Using a density fluctuation model (deduced from observations of solar radio bursts and angular broadening of extra-solar sources) we then deduce the magnitudes of the flow velocities (and/or phase speeds) required to produce the observed frequency broadenings. The inferred speeds are compared with other characteristic speeds, such as the sound speed, the Alfvén speed, and the solar wind speed.

Sections 6 and 7 compare the power supplied by large-scale Alfvénic kink/shearing motions with the heating effected by damping of the ion-sound waves associated with density fluctuations at much shorter length scales. In Section 8 we summarize the results obtained and present our conclusions. A number of Appendices present some of the more tedious mathematical derivations of certain results.

## 2. STATIC DENSITY FLUCTUATIONS AND ANGULAR BROADENING

Density fluctuations with wavevector  $\mathbf{q}$  are characterized by their three-dimensional wavevector spectrum  $S(\mathbf{q})$ , typically normalized (see, e.g., Kontar et al. 2023) by the rms level of fluctuations in the local density  $n \text{ (cm}^{-3}\text{)}$ :

$$\int S(\mathbf{q}) \frac{d^3 q}{(2\pi)^3} = \frac{\langle \delta n^2 \rangle}{n^2} \equiv \epsilon^2 . \quad (1)$$

Following previous studies (e.g., Arzner & Magun 1999; Bian et al. 2019; Kontar et al. 2019), the diffusion tensor describing elastic scattering of radio waves with wavevector  $\mathbf{k}$  in a medium containing static density fluctuations can be written as

$$D_{ij} = \frac{\pi \omega_{pe}^4}{4 \omega^2} \int q_i q_j S(\mathbf{q}) \delta(\mathbf{q} \cdot \mathbf{v}_g) \frac{d^3 q}{(2\pi)^3} , \quad (2)$$

where  $q_i, q_j \text{ (cm}^{-1}\text{)}$  are the components of the density fluctuation wavevector in the directions labeled by the suffices  $i, j$ , the wave group velocity  $\mathbf{v}_g = \partial \omega / \partial \mathbf{k}$  and  $\omega(\mathbf{k}) = (\omega_{pe}^2 + c^2 k^2)^{1/2}$  is the angular frequency of electromagnetic waves with wavevector  $\mathbf{k}$  in a plasma with local plasma frequency  $\omega_{pe}(\mathbf{r})$ .

Similar to Kontar et al. (2023), we take the spectrum of density turbulence to be anisotropic with a constant anisotropy factor  $\alpha$ , so that

$$S(\mathbf{q}) = S(\tilde{q}) , \quad \text{where} \quad \tilde{q} = \sqrt{\frac{q_\parallel^2}{\alpha^2} + q_{\perp 2}^2 + q_{\perp 1}^2} , \quad (3)$$

which has axial symmetry around the  $\parallel$  direction, i.e., along the magnetic field  $\mathbf{B}$ , and is isotropic with respect to the  $\tilde{\mathbf{q}}$  basis. In matrix form,  $\tilde{\mathbf{q}} = \mathbf{A} \mathbf{q} = (\alpha^{-1} q_{\parallel}, q_{\perp_2}, q_{\perp_1})$ , where  $\mathbf{A}$  is the anisotropy matrix

$$\mathbf{A} = \begin{pmatrix} \alpha^{-1} & 0 & 0 \\ 0 & 1 & 0 \\ 0 & 0 & 1 \end{pmatrix}. \quad (4)$$

The quantity  $\alpha$  appearing in Equations (3) and (4) quantifies the degree of anisotropy in the turbulence distribution:  $\alpha < 1$  corresponds to density fluctuations elongated along the magnetic field ( $q_{\parallel}^{-1} > q_{\perp}^{-1}$ , i.e.,  $q_{\parallel} < q_{\perp}$ ), as is often observed in the solar wind (e.g., [Celnikier et al. 1987](#); [Musset et al. 2021](#)). Typical reported values of  $\alpha$  are 0.1 – 0.4 (e.g., [Dennison & Blesing 1972](#); [Coles & Harmon 1989](#); [Armstrong et al. 1990](#); [Kontar et al. 2019](#); [Chen et al. 2020](#); [Kuznetsov et al. 2020](#); [Clarkson et al. 2023](#)).

For a radio wave propagating with  $\mathbf{v}_g \simeq c \mathbf{k}/|\mathbf{k}|$  along the  $\perp_1$ -direction (see Figure 5), we can find the components of the diffusion tensor elements, viz. (Equation (A5))

$$\mathbf{D} = \frac{\pi \omega_{pe}^4}{16 \omega^2 c} \overline{q \epsilon^2} \begin{pmatrix} \alpha^2 & 0 & 0 \\ 0 & 1 & 0 \\ 0 & 0 & 0 \end{pmatrix}, \quad (5)$$

where we have introduced the spectrum-weighted mean wavenumber  $\overline{q \epsilon^2}$ , defined as ([Kontar et al. 2023](#))

$$\overline{q \epsilon^2} = \int q S(q) \frac{d^3 q}{(2\pi)^3} = \alpha \int \tilde{q} S(\tilde{q}) \frac{d^3 \tilde{q}}{(2\pi)^3} = \alpha \frac{4\pi}{(2\pi)^3} \int \tilde{q}^3 S(\tilde{q}) d\tilde{q}. \quad (6)$$

where in the second equality, we have transformed from the  $\mathbf{q}$  basis to the  $\tilde{\mathbf{q}}$  basis, in which the wavenumber spectrum is isotropic.

The diffusion tensor  $\mathbf{D}$  given by Equation (5) has two non-zero elements that determine the scattering rates  $d\langle \Delta k_{\parallel}^2 \rangle / dt$  and  $d\langle \Delta k_{\perp_2}^2 \rangle / dt$ . The  $\perp_2$  and  $\parallel$  directions are perpendicular to the wave propagation vector  $\mathbf{k}$  (see Figure 5 in Appendix A). For  $\Delta \mathbf{k} \perp \mathbf{k}$ , the scattering corresponding to terms  $d\langle \Delta k_{\parallel}^2 \rangle / dt$  and  $d\langle \Delta k_{\perp_2}^2 \rangle / dt$  is elastic:  $|\mathbf{k} + \Delta \mathbf{k}|^2 \simeq |\mathbf{k}|^2 + 2\mathbf{k} \cdot \Delta \mathbf{k} = |\mathbf{k}|^2$ , i.e.,  $|\mathbf{k}|$  is a constant. To change the absolute value of  $|\mathbf{k}|$ , or equivalently the wave frequency  $\omega(\mathbf{k}) \simeq c|\mathbf{k}|$ , we must have non-zero  $\mathbf{k} \cdot \Delta \mathbf{k}$ , i.e.  $d\langle \Delta k_{\perp_1}^2 \rangle / dt \neq 0$ . The effects of such inelastic scatterings, which are important for frequency broadening, are next considered.

### 3. INELASTIC SCATTERING OF RADIO WAVES

When the density fluctuations are not static, but are instead due to either waves or density fluctuations advected by plasma motions, the scattering could be inherently inelastic with  $d\langle \Delta k_{\perp_1}^2 \rangle / dt \neq 0$ , so that  $|\mathbf{k}| \neq \text{const}$ , leading to a change in the wave frequency  $\omega$ . Consider an electromagnetic (EM) wave with energy  $\omega(\mathbf{k})$  and wavevector  $\mathbf{k}$  that is scattered by a density fluctuation with wavenumber  $\mathbf{q}$  and frequency  $\Omega(\mathbf{q})$ , resulting in a scattered EM wave with frequency  $\omega(\mathbf{k}')$  and wavevector  $\mathbf{k}'$ . Momentum and energy conservation in such a three-wave process ([Tsytovich & ter Haar 1995](#)) demands that

$$\mathbf{k} + \mathbf{q} = \mathbf{k}', \quad \omega(\mathbf{k}) + \Omega(\mathbf{q}) = \omega(\mathbf{k}'). \quad (7)$$

Using the dispersion relation for electromagnetic waves  $\omega^2(\mathbf{k}) = \omega_{pe}^2 + c^2 k^2$  and using the resonance condition  $\Omega(\mathbf{q}) = \mathbf{v} \cdot \mathbf{q}$  as a dispersion relation, one finds that, for  $\omega \gg \omega_{pe}$ ,  $|\mathbf{k}| \gg |\mathbf{q}|$ , and  $|\mathbf{k}'| \gg |\mathbf{q}|$ ,

$$\mathbf{q} \cdot \frac{\mathbf{k}}{|\mathbf{k}|} \simeq \frac{\Omega(\mathbf{q})}{c} = \frac{\mathbf{q} \cdot \mathbf{v}}{c} . \quad (8)$$

Hence to satisfy the conservation of energy and momentum relations (7), the density wavevector  $\mathbf{q}$  should be quasi-perpendicular to  $\mathbf{k}$ :

$$\frac{q_{\parallel \mathbf{k}}}{q_{\perp \mathbf{k}}} \simeq \frac{v_{\perp \mathbf{k}}}{c} \ll 1 , \quad (9)$$

showing that density fluctuations involving motions perpendicular to  $\mathbf{k}$  ( $v_{\perp \mathbf{k}} \neq 0$ ) produce a shift in the the magnitude  $|\mathbf{k}|$  of the electromagnetic wavevector and hence in the frequency of the electromagnetic wave.

### 3.1. Radially moving density fluctuations

The generalization of Equation (2) in the presence of non-static density fluctuations is

$$D_{ij} = \frac{\pi \omega_{pe}^4}{4 \omega^2} \int q_i q_j S(\mathbf{q}) \delta(\Omega(\mathbf{q}) - \mathbf{q} \cdot \mathbf{v}_g) \frac{d^3 q}{(2\pi)^3} , \quad (10)$$

where  $\Omega(\mathbf{q})$  is the dispersion relation for the density fluctuations, which is conceptually identical to plasma wave scattering on plasma density fluctuations (Sagdeev & Galeev 1969; Goldman & Dubois 1982; Ratcliffe et al. 2012).

We first consider density fluctuations moving along the radial direction  $\mathbf{B}$ , i.e.,  $\Omega(\mathbf{q}) = v_{\parallel} q_{\parallel}$ . In this case, the change of frequency (or absolute value of the wavevector of the radio wave) is due to non-zero values of  $v_{\parallel}$ . One can include the effects of the moving waves in the calculation of the components  $D_{ij}$  of the diffusion tensor that affects both the direction of propagation (angular broadening) and change in wavenumber (frequency broadening). As shown in Equation (B14), the modified diffusion tensor takes the form

$$D = \frac{\pi \omega_{pe}^4}{16 \omega^2 c} \overline{q \epsilon^2} \begin{pmatrix} \alpha^2 & 0 & 0 \\ 0 & 1 & 0 \\ 0 & 0 & \frac{\alpha^2 v_{\parallel}^2}{c^2} \end{pmatrix} . \quad (11)$$

Naturally, Equation (11) reduces to Equation (5) when  $v_{\parallel} \rightarrow 0$ .

### 3.2. Transverse density fluctuations

We can similarly evaluate the diffusion tensor components  $D_{ij}$  for the case of waves moving in the perpendicular (transverse) direction, with assumed dispersion relation  $\Omega(\mathbf{q}) = v_{\perp 2} q_{\perp 2}$ . Substituting this into Equation (10) gives the form of the diffusion tensor (see Equation (B19))

$$D = \frac{\pi \omega_{pe}^4}{16 \omega^2 c} \overline{q \epsilon^2} \begin{pmatrix} \alpha^2 & 0 & 0 \\ 0 & 1 & 0 \\ 0 & 0 & \frac{v_{\perp 2}^2}{c^2} \end{pmatrix} , \quad (12)$$

Equations (11) and (12) show that all motions in the plane of the sky, i.e., perpendicular to the radio wave propagation direction, lead to a change in the absolute magnitude of the radio-wave wavenumber. If there are waves in both the parallel ( $\parallel$ ) and perpendicular ( $\perp_2$ ) directions, the diffusion effects simply add together:

$$D = \frac{\pi \omega_{pe}^4}{16 \omega^2 c} \overline{q \epsilon^2} \begin{pmatrix} \alpha^2 & 0 & 0 \\ 0 & 1 & 0 \\ 0 & 0 & \frac{\alpha^2 v_{\parallel}^2 + v_{\perp_2}^2}{c^2} \end{pmatrix}. \quad (13)$$

We note that since  $\alpha < 1$  perpendicular motions are more effective at frequency broadening than radial (parallel) motions.

### 3.3. Random (turbulent) motions

Observation of solar corona UV spectral lines often show significant broadening in excess of the thermal width at which the responsible atomic species is formed (e.g., Hassler et al. 1990; Chandrasekhar et al. 1991; Banerjee et al. 1998; Doyle et al. 1998, 1999; Esser et al. 1999; Contesse et al. 2004; Banerjee et al. 2009; Landi & Cranmer 2009; Singh et al. 2011). Such non-thermal broadening of lines is normally interpreted as the unresolved motion of emitting ions: either fluid motions (unresolved flows or waves) or motion of accelerated non-thermal ions (e.g. Jeffrey et al. 2014). Large-scale fluid motions lead to resonance broadening (e.g., Bian et al. 2012; Wilczek & Narita 2012). Considering first random motions in the transverse ( $\perp_2$ ) direction, we suggest that the small scale density fluctuations (mostly near the inner scale  $q_i^{-1}$  of density turbulence responsible for radio-wave scattering; Kontar et al. 2023) are advected by large-scale random plasma motions with speeds corresponding to the outer scale of the turbulence. Within this framework, the velocity fluctuations  $\langle v_{\perp_2}^2 \rangle$  have a line broadening effect that is identical to that of non-thermal ion velocities, and so can be modeled by replacing the Dirac delta-function resonance condition by a finite-width Gaussian characterized by a turbulent velocity  $v_{\perp}$ :

$$\delta(\Omega(\mathbf{q}) - \mathbf{q} \cdot \mathbf{v}_g) \rightarrow \frac{1}{\sqrt{2\pi q_{\perp_2}^2 \langle v_{\perp_2}^2 \rangle}} \exp \left[ -\frac{(\Omega(\mathbf{q}) - \mathbf{q} \cdot \mathbf{v}_g)^2}{2 q_{\perp_2}^2 \langle v_{\perp_2}^2 \rangle} \right], \quad (14)$$

where  $\langle v_{\perp_2}^2 \rangle$  is the variance of large-scale motion velocities. This is an application of a random sweeping hypothesis (Tennekes 1975) to radio scattering measurements.

The presence of random motions superimposed on the large-scale flows thus gives diffusion tensor components

$$D_{ij} = \frac{\pi \omega_{pe}^4}{4 \omega^2} \int q_i q_j S(\mathbf{q}) \frac{1}{\sqrt{2\pi q_{\perp_2}^2 \langle v_{\perp_2}^2 \rangle}} \exp \left[ -\frac{(\Omega(\mathbf{q}) - \mathbf{q} \cdot \mathbf{v}_g)^2}{2 q_{\perp_2}^2 \langle v_{\perp_2}^2 \rangle} \right] \frac{d^3 q}{(2\pi)^3}. \quad (15)$$

Integrating in the approximation  $q_{\perp_2}^2 \langle v_{\perp_2}^2 \rangle \ll q^2 c^2$  and taking  $\Omega = 0$  we obtain (Equation (C24)) the diffusion tensor



$$D = \frac{\pi \omega_{pe}^4}{16 \omega^2 c} \overline{q \epsilon^2} \begin{pmatrix} \alpha^2 & 0 & 0 \\ 0 & 1 & 0 \\ 0 & 0 & \frac{\langle v_{\perp 2}^2 \rangle}{c^2} \end{pmatrix} \quad (16)$$

leading to a frequency broadening that is mathematically similar to Equation (12), but where  $\langle v_{\perp 2}^2 \rangle$  now represents random velocity fluctuations.

Similar considerations apply to random motions in the parallel (i.e., radial) direction, with a factor of  $\alpha^2$  applied, so that if there are random motions in both directions,

$$D = \frac{\pi \omega_{pe}^4}{16 \omega^2 c} \overline{q \epsilon^2} \begin{pmatrix} \alpha^2 & 0 & 0 \\ 0 & 1 & 0 \\ 0 & 0 & \frac{\alpha^2 \langle v_{\parallel}^2 \rangle + \langle v_{\perp 2}^2 \rangle}{c^2} \end{pmatrix}. \quad (17)$$

Again, since  $\alpha < 1$ , perpendicular motions are more effective at frequency broadening than radial (parallel) motions.

#### 4. OBSERVED FREQUENCY BROADENING

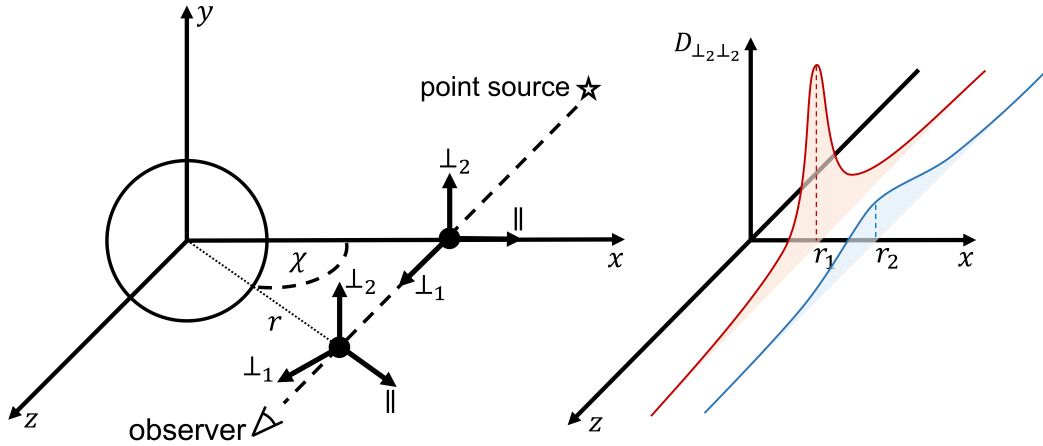


**Figure 1.** The left panel shows the Sun-centered coordinate system and its relation to heliocentric distance and the line of sight from a distant point source. The broadening of point sources is calculated as an integral along  $z$ . The right-hand panel qualitatively shows how the  $D_{\perp_1 \perp_2}$  diffusion tensor component (see e.g., Equation (5)) varies along  $z$ , as illustrated for sources at two different heliocentric distances  $r(z = 0)$ , with  $r_1 < r_2$ .

To compare with the observations, we note that radio wave with wavevector  $\mathbf{k}$  is propagating along the  $z$ -direction. We assign the  $\parallel$  direction with the (assumed radial) solar magnetic field  $\mathbf{B}$  (Figure 1). We also assign the  $\perp_1$  direction to the perpendicular direction that is aligned with the wave propagation direction at  $z = 0$ , and  $\perp_2$  to the perpendicular direction that is orthogonal to both  $\parallel$  and  $\perp_1$ , i.e., perpendicular to the projection of the radial direction on the plane of the sky. The right-handed ( $\parallel, \perp_2, \perp_1$ ) coordinate system is obtained by rotating the  $(x, y, z)$  coordinate system by an angle  $(-\chi)$  around the  $y$ -axis (Figure 1).

Analogously to the results from the three previous subsections, the variance of the wavenumber  $k$  along the path of the radio wave due to motions in the plane of the sky (here denoted by  $v_{\perp\mathbf{k}}$ ) in the solar atmosphere can be written as

$$\frac{d\langle k_z^2 \rangle}{dt} = 2D_{zz} = \frac{\pi\omega_{pe}^4}{8\omega^2 c} \frac{\alpha^2 \langle v_{\parallel}^2 \rangle \cos^2 \chi + \langle v_{\perp 2}^2 \rangle + \langle v_{\perp 1}^2 \rangle \sin^2 \chi}{c^2}, \quad (18)$$

where  $\chi(z)$  is the angle between the radial direction of the magnetic field and the  $x$ -axis (see Figure 1). For perpendicular motions that are dominated by gyrotropic turbulence,  $\langle v_{\perp 1}^2 \rangle = \langle v_{\perp 2}^2 \rangle = \langle v_{\perp}^2 \rangle$ , this can be written as

$$\frac{d\langle k_z^2 \rangle}{dt} = \frac{\pi\omega_{pe}^4}{8\omega^2 c} \frac{v_{\perp\mathbf{k}}^2}{c^2}, \quad (19)$$

where

$$v_{\perp\mathbf{k}}^2 = \sqrt{\alpha^2 \langle v_{\parallel}^2 \rangle \cos^2 \chi + \langle v_{\perp}^2 \rangle (1 + \sin^2 \chi)} \quad (20)$$

represents the weighted sum of all motions perpendicular to  $\mathbf{k}$ , i.e., in the  $(x, y)$  plane of the sky, and the  $\langle v_{\parallel}^2 \rangle$  term is the sum in quadrature of both steady flows and random velocities in the parallel direction. Both random motions and oscillations with the same phase speed contribute at the same level. Such motions and/or oscillations of density fluctuations in the plane of the sky are perpendicular to the direction of radio wave propagation  $\mathbf{k}$ ; they hence lead to a change in wavenumber  $\Delta\mathbf{k}$  that is aligned with  $\mathbf{k}$  and so to a change in the magnitude  $|\mathbf{k}|$ , i.e., to frequency broadening. In the limit  $\omega \gg \omega_{pe}$ , the group velocity of the radio wave  $\mathbf{v}_{gr} = \partial\omega/\partial\mathbf{k} = c^2 \mathbf{k}/\omega \simeq c$ . The frequency broadening rates per unit travel distance  $v_{gr} dt$  along the direction of propagation  $z$  can be written (similarly to Kontar et al. 2023) as

$$\frac{\langle \Delta f^2 \rangle}{f^2} = \int_{los} \frac{1}{k_z^2} \frac{d\langle k_z^2 \rangle}{c dt} dz = \int_{los} \frac{\pi}{8} \frac{v_{\perp\mathbf{k}}^2}{c^2} \frac{\omega_{pe}^4}{\omega^4} \overline{q \epsilon^2}(r) dz, \quad (21)$$

which can be integrated for known  $v_{\perp\mathbf{k}}^2$ . The right panel of Figure 2 shows the predicted (taking  $n^2 \overline{q \epsilon^2}$  from Kontar et al. 2023) broadening for a typical perpendicular speed  $v_{\perp} = 30 \text{ km s}^{-1}$  from non-thermal line measurements, and  $v_{\parallel} = \sqrt{v_s^2 + v_{sw}^2}$  where the sound speed  $v_s$  is given by Equation (25) and the solar wind speed  $v_{sw}$  is given by Equation (26). Importantly, the result does not depend on density model, but on the strength of density fluctuations  $n^2 \overline{q \epsilon^2}$  and the plasma velocities.

Equation (21) can be also written approximately as in Appendix F or noting that the largest contribution to frequency broadening comes from the high density region near  $z = 0$  (Figure 1), and hence, to a good approximation, we can take  $\chi \simeq 0$  in equation (21). Thus, we can write  $v_{\perp\mathbf{k}}^2 \simeq \alpha^2 \langle v_{\parallel}^2 \rangle + \langle v_{\perp}^2 \rangle$  taking values at  $z = 0$ . The frequency broadening integrated over the path of the radio wave is now given by

$$\frac{\langle \Delta f^2 \rangle}{f^2} \simeq \frac{\pi}{8} \frac{v_{\perp\mathbf{k}}^2}{c^2 \omega^4} \int_{los} \omega_{pe}^4 \overline{q \epsilon^2} dz = \frac{2\pi^3 e^4}{m_e^2 c^2 \omega^4} v_{\perp\mathbf{k}}^2 \int_{los} n^2 \overline{q \epsilon^2} dz; \quad (22)$$

i.e.,



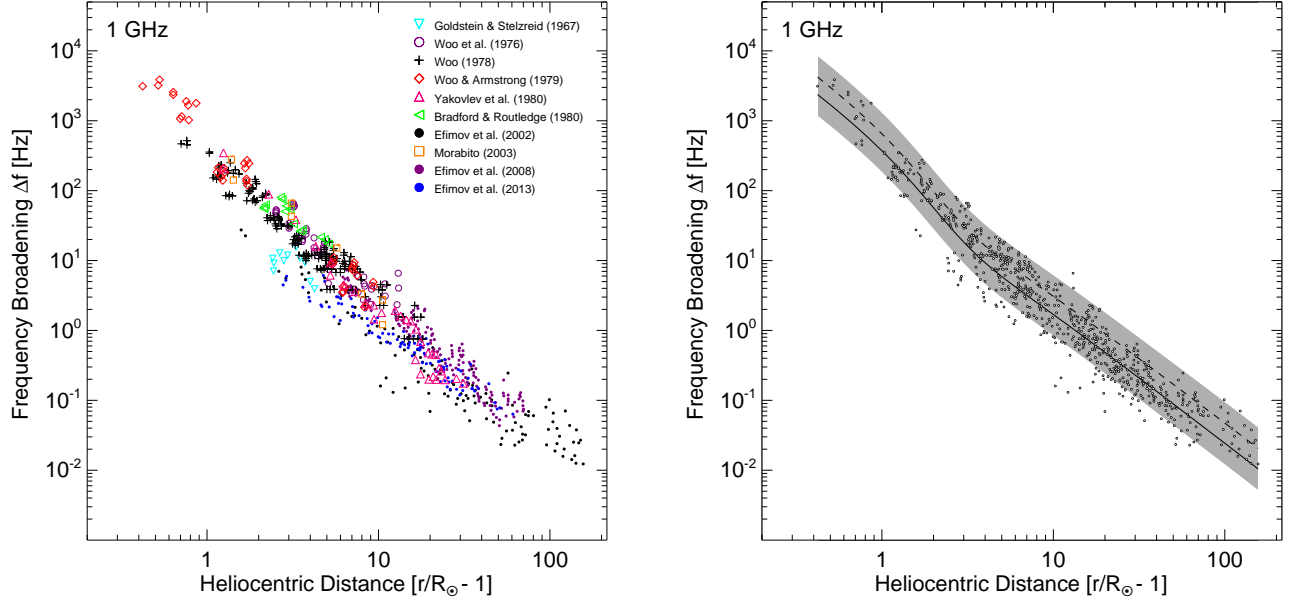


**Figure 2.** **Left:** Observed spectral broadening  $\Delta f = \sqrt{\langle \Delta f^2 \rangle}$  (the square root of the variance) of spacecraft signals observed through the corona from various studies, where each carrier signal is scaled to  $f = 1$  GHz using  $\Delta f/f \propto 1/f^2$ . The conversions applied to the different measures to retrieve the standard deviation are noted in Appendix D. **Right:** Form of  $\Delta f$  derived from Equations (20) and (21), for  $v_{\perp} = 30 \text{ km s}^{-1}$  (from the non-thermal line broadening measurements in Appendix E), and  $v_{\parallel} = \sqrt{v_s^2 + v_{\text{sw}}^2}$ , where the sound speed  $v_s$  is given by Equation (25) and the solar wind speed  $v_{\text{sw}}$  is given by Equation (26). The solid and dashed lines show  $\Delta f$  derived using  $1 \times \overline{q \epsilon^2}$  for  $\alpha = 0.25$  and  $\alpha = 0.4$ , respectively, while the grey area shows the range in  $\Delta f$ . The lower bound is given by  $1/2 \times \overline{q \epsilon^2}$  for  $\alpha = 0.25$ , and the upper bound is given by  $2 \times \overline{q \epsilon^2}$  for  $\alpha = 0.4$ .

$$\frac{\Delta f}{f} \simeq \frac{1}{(8\pi)^{1/2}} \left( \frac{e^2}{m_e c} \right) \left( \int_{\text{los}} n^2 \overline{q \epsilon^2} dz \right)^{1/2} \frac{v_{\perp \mathbf{k}}}{f^2}. \quad (23)$$

which shows that the fractional frequency broadening  $\Delta f/f$  depends on the carrier frequency  $f$  as  $1/f^2$  and is determined by motions in the plane of the sky. Although both parallel and perpendicular velocities may be present, the parallel velocities (both steady flows and random motions) are weighted by the anisotropy parameter  $\alpha < 1$  (cf. the expression for frequency broadening in an isotropic plasma; Equation (36) of [Bian et al. 2019](#)). Knowing the anisotropy factor  $\alpha$  and the  $n^2 \overline{q \epsilon^2}(z)$  density fluctuation profile from independent measurements, one can deduce the characteristic speeds of density fluctuations using Equation (23). Indeed, using an analytic approximation for  $n^2 \overline{q \epsilon^2}$  derived from solar observations ([Kontar et al. 2023](#)), one can find an approximate analytical expression for  $\Delta f$ , which is presented in Appendix F.

## 5. FREQUENCY BROADENING MEASUREMENTS

Frequency broadening observations (for details see Appendix D) have been conducted a number of times using signals from different spacecraft ([Goldstein & Stelzried 1967](#); [Woo et al. 1976](#); [Woo 1978](#); [Woo & Armstrong 1979](#); [Bradford & Routledge 1980](#); [Yakovlev et al. 1980](#); [Efimov et al. 2002](#);

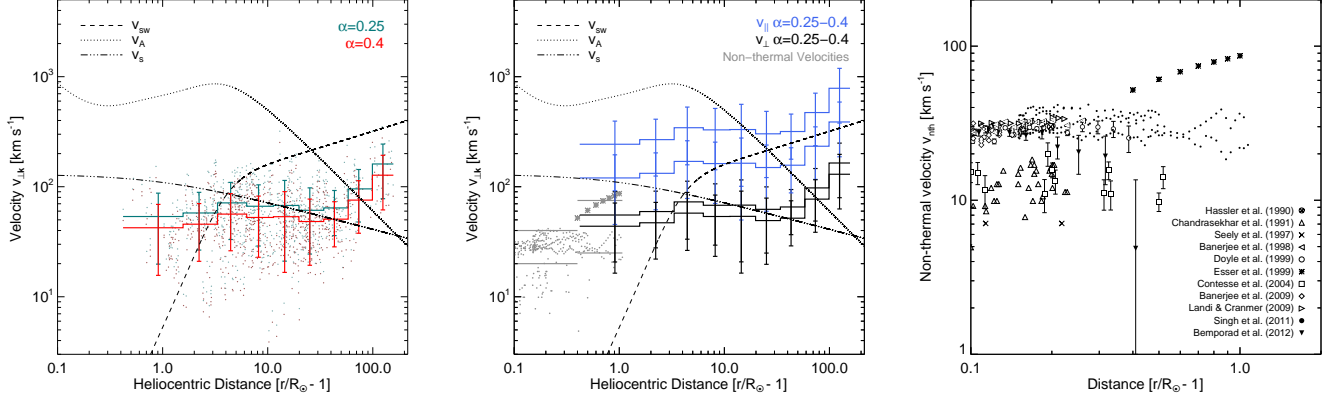


**Figure 3.** **Left:** Plane-of-sky velocity  $v_{\perp k}$  calculated using frequency broadening measurements from Figure 2, Equation (24), and the  $n^2 \bar{q} \epsilon^2$  values at various distances  $r$  derived from measurements of other phenomena, such as angular broadening of extra-solar sources and the location, size and timing of solar radio bursts (Kontar et al. 2023). The green and red points show the conversion of individual  $\Delta f$  data points from Figure 2, for different values of  $\alpha$ , with binned averages and weighted uncertainties on each bin. **Middle:** Parallel and perpendicular velocities  $v_{\parallel}$  (blue) and  $v_{\perp}$  (black) required to solely explain the frequency broadening measurements in Figure 2. The grey dots and stars show a summary of the measured values of the non-thermal velocity standard deviation from the right panel. Also shown is the solar wind speed  $v_{SW}$  (Equation (26)), the ion-sound speed  $v_s$  (Equation (25)), and the Alfvén speed from Equation (27), obtained using the density and magnetic field models in Equations (A1) and (A2) of Kontar et al. (2023). **Right:**  $1\sigma$  non-thermal velocities  $v_{nth}$  from line-of-sight Doppler broadening of coronal lines (see Appendix E for details).

Morabito et al. 2003; Efimov et al. 2008, 2013). The left panel of Figure 2 shows the compilation of  $1\sigma$  frequency broadening (the square root of the variance,  $\Delta f \equiv \sqrt{\langle \Delta f^2 \rangle}$ ) of spacecraft signals as a function of heliocentric distance. For observation at different frequencies, the broadened quantity is scaled to 1 GHz using  $\Delta f_{1\text{GHz}} = \Delta f_{\text{obs}} (f_{\text{obs}}[\text{GHz}])^2$ . Appendix D provides information on the conversion of other reported broadening measures. The trend of  $\Delta f$  with heliocentric distance follows a broken power-law, with a steeper power law index  $\sim -2$  below  $\sim 3 R_{\odot}$ , transitioning to a somewhat flatter power-law index of approximately  $-1.7$  above  $\sim 10 R_{\odot}$ .

Instead of assuming a flow (or turbulent) velocity value, we can alternatively use the measured frequency broadenings to determine the associated velocity, by rewriting Equation (23) in the form

$$v_{\perp k} \equiv \sqrt{\alpha^2 \langle v_{\parallel}^2 \rangle + \langle v_{\perp}^2 \rangle} \simeq \frac{(8\pi)^{1/2}}{c r_o} \frac{f^2}{\left( \int_{\text{los}} n^2 \bar{q} \epsilon^2 dz \right)^{1/2}} \frac{\Delta f}{f}, \quad (24)$$

where  $r_o = e^2/m_e c^2$  is the classical electron radius and is evaluated taking  $n(r[z]) \bar{q} \epsilon^2(r[z])$  from Kontar et al. (2023). In the left panel of Figure 3 we show  $v_{\perp k}$  (in  $\text{km s}^{-1}$ ) as a function of heliocentric distance  $r$ , for two different values of the anisotropy parameter  $\alpha$ . Further, by taking  $v_{\perp} = 0$  or  $v_{\parallel} = 0$ , one can obtain an upper limit on the magnitude of the remaining component of  $v_{\perp k}$ . The middle panel of Figure 3 compares these maximum values of  $v_{\parallel}$  and  $v_{\perp}$  with various other speeds, including the solar wind speed  $v_{SW}$ , the sound speed  $v_s$ , the Alfvén speed  $v_A$ , and nonthermal velocities deduced from UV spectral line broadening observations. These reference speeds are calculated as follows:

- *Sound speed:* The electron temperature of the solar wind is observed to decrease with heliocentric distance:  $T_e \propto r^{-(0.3-0.7)}$  (e.g., [Stverak et al. 2015](#)). If we model the temperature as  $T_e \simeq 2 \times 10^6 (r/R_\odot - 1)^{-0.5}$  K, then the sound speed  $v_s \simeq \sqrt{k_B T_e / m_i}$  varies with heliocentric distance  $r$  as

$$v_s(r) \simeq 130 \left( \frac{r}{R_\odot} - 1 \right)^{-0.25} \text{ km s}^{-1} . \quad (25)$$

- *Solar wind speed:* In the spherically symmetric expanding corona ([Parker 1958](#)), mass conservation  $v_{sw} r^2 n(r) = \text{const}$  requires that, with a typical solar wind speed of  $400 \text{ km s}^{-1}$  at 1 au,

$$v_{sw}(r) \approx 400 \left( \frac{n(1 \text{ au})}{n(r)} \right) \left( \frac{1 \text{ au}}{r} \right)^2 \text{ km s}^{-1} , \quad (26)$$

where  $n(r)$  is the plasma density.

- *Alfvén speed:* The Alfvén speed

$$v_A(r) = \frac{B(r)}{\sqrt{4\pi m_i n(r)}} \quad (27)$$

is obtained using the magnetic field and density models in Equations (A1) and (A2) of [Kontar et al. \(2023\)](#).

- *Nonthermal velocities:* Nonthermal turbulent velocities are inferred through measurement of the excess width of EUV coronal spectral lines compared to their thermal widths, and are often interpreted as evidence of perpendicular velocity fluctuations at speeds of a few tenths of the Alfvén speed (e.g., [Doyle et al. 1998](#); [Singh et al. 2011](#)). The inferred turbulent velocities are dependent on the assumed ion temperature ([Seely et al. 1997](#)). Measurement of the width of spectral lines in the radio domain also provide a (temperature-independent) measure of velocity fluctuations. Figure 3 also shows various measurements of  $1\sigma$  nonthermal velocities at different heliocentric distances; this information is also summarized in the middle panel of Figure 3.

The middle panel of Figure 3 shows clearly that the velocities deduced from frequency broadening measurements become dominated by the solar wind speed at large heliocentric distances  $r > 10 R_\odot$ . However, closer to the Sun at  $r \lesssim 10 R_\odot$ , the solar wind speed contribution is much smaller than the inferred  $v_{\perp k}$  speeds, whether radial velocities  $v_{\parallel}$  in the range  $(100-300) \text{ km s}^{-1}$ , or perpendicular motions  $v_{\perp}$  in the range  $(25-75) \text{ km s}^{-1}$ , or a combination of such motions are considered. Both these inferred speed ranges are well below the Alfvén speed; however, perpendicular motions of this magnitude are quite consistent with the nonthermal speeds deduced from the observed widths of UV spectral lines. The next section discusses such nonthermal turbulent motions and their possible role in coronal heating.

## 6. VELOCITY FLUCTUATIONS AND ALFVÉN WAVE CASCADE

Velocity fluctuations (non-thermal velocities of emitting ions) along of line of sight are often interpreted as manifestations of perpendicular to magnetic field velocities (e.g., [Doyle et al. 1998](#)) and (as

we have seen above) frequency broadening of radio signals. Such motions are commonly interpreted as Alfvén waves, which can undergo turbulent cascade to smaller scales (e.g., [Hollweg 1978](#); [Leer et al. 1982](#); [Goldstein et al. 1995](#); [Tu & Marsch 1995](#)). The power per unit mass ( $\text{erg g}^{-1} \text{s}^{-1}$ ) available to be deposited through such a Kolmogorov cascade in strong MHD turbulence ([Goldreich & Sridhar 1995](#)) is estimated to be

$$\epsilon_{\ell_{\perp}} \simeq \frac{v_{\perp}^2}{\tau} \simeq \frac{v_{\perp}^3}{\ell_{\perp}} , \quad (28)$$

where the characteristic cascade time is  $\tau = \ell_{\perp}/v_{\perp}$ , with  $\ell_{\perp}$  being a measure of the transverse correlation length ([Hollweg 1986](#)). Although  $\ell_{\perp}$  is not measurable directly in the corona, one can assume it to be comparable to the transverse size of a flux tube (see Equation (4) in [Hollweg 1986](#)):

$$\ell_{\perp} = \frac{7.5 \times 10^8}{\sqrt{B}} \text{ cm} , \quad (29)$$

where  $B$  is in Gauss. This is also similar to the estimate used in MHD simulations (see Equation (51) in [Cranmer & van Ballegooijen 2005](#), and subsequent discussion therein).

The quantity  $\epsilon_{\ell_{\perp}}$  is the power per unit mass at the outer scale of the inertial range; it is the rate at which energy enters the turbulent cascade process at the largest scales, and it is a scale-invariant quantity within the inertial range of turbulence. The value of  $\epsilon_{\ell_{\perp}}$  often serves as a measure of coronal heating via Alfvén turbulent cascade, or the specific energy rate associated with anisotropic MHD turbulence ([Goldreich & Sridhar 1995](#)). This energy input rate plays a role that is conceptually similar to the solar flare scenario, in which an Alfvén turbulence cascade (estimated from measured non-thermal velocities) is believed to power particle acceleration in solar flares ([Kontar et al. 2017a](#); [Stores et al. 2021](#)).

The left panel of Figure 4 shows the values of  $\epsilon_{\ell_{\perp}}$  deduced from the perpendicular velocities inferred from radio wave frequency broadening observations (Figure 3). They suggest an energy cascade rate  $\epsilon_{\ell_{\perp}} \simeq 10^{11} \text{ erg g}^{-1} \text{ s}^{-1}$ , a value that is similar to earlier estimates (e.g., [Hollweg 1986](#); [Cranmer & van Ballegooijen 2005](#)).

## 7. DAMPING OF ION-SOUND WAVES

Energy could be supplied to the corona and solar wind via absorption of the energy contained in ion-sound or slow magneto-sonic waves (e.g., [Kellogg 2020](#), and references therein), that are often observed in the corona (e.g., [DeForest & Gurman 1998](#); [Wang et al. 2009](#); [Gupta et al. 2012](#)) and solar wind close to the Sun ([Zank et al. 2024](#)). For  $q \lambda_{De} \ll 1$  (where  $\lambda_{De}$  is the Debye length), the spectral energy density of parallel propagating ion-sound waves  $W_q$  ( $\text{erg cm}^{-3} [\text{cm}^{-1}]^{-3}$ ) is related to the spectrum of density fluctuations  $S(q)$  ( $[\text{cm}^{-1}]^{-3}$ ) by (see, e.g., Appendix C in [Lyubchik et al. 2017](#))

$$\frac{W_q^s}{n_e k_B T_e} \simeq \frac{|\delta n_e|_q^2(q)}{n_e^2} \equiv S(q) . \quad (30)$$

Parallel propagating ion-sound waves are strongly damped, especially in the plasma with  $T_i \simeq T_e$ . The Landau damping rate  $\gamma_q^s$  ( $\text{s}^{-1}$ ) of ion-sound waves with  $v_s \simeq \sqrt{k_B T_e / m_i}$  is proportional to the wave frequency  $\Omega_q^s = v_s q_{\parallel}$  (e.g., [Krall & Trivelpiece 1973](#); [Pécsele 2012](#)):

$$\gamma_q^s = \sqrt{\frac{\pi}{8}} \Omega_q^s \left\{ \sqrt{\frac{m_e}{m_i}} + \left( \frac{T_e}{T_i} \right)^{3/2} \exp \left[ - \left( \frac{T_e}{2T_i} \right) \right] \right\} , \quad (31)$$

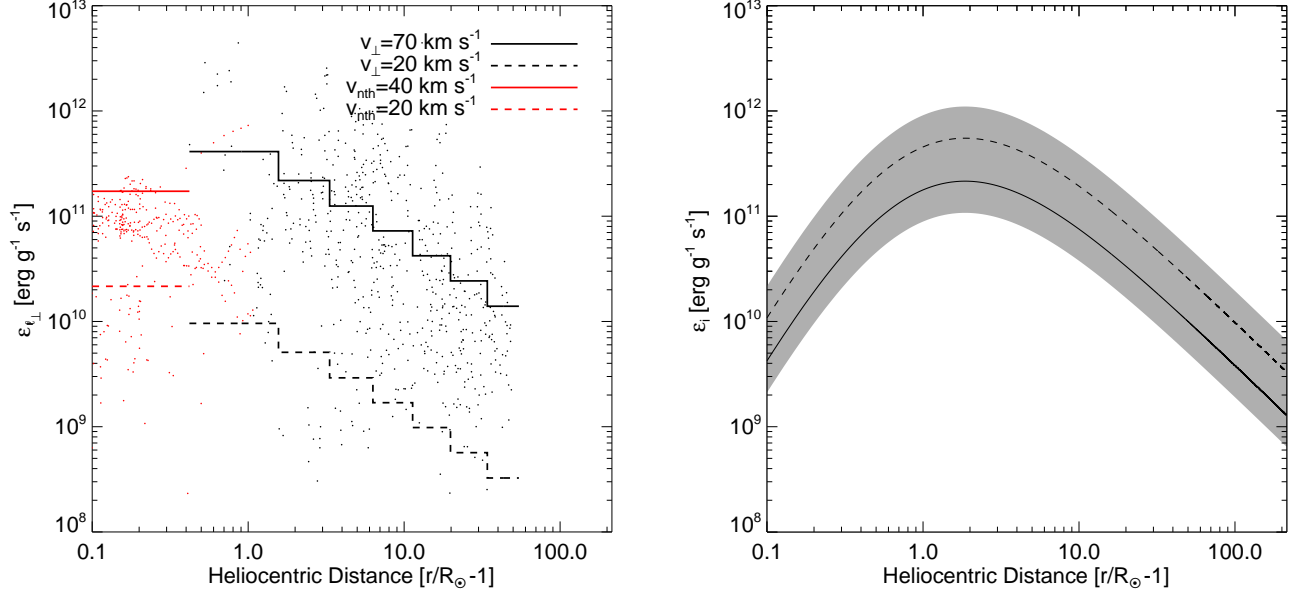


**Figure 4. Left:** Available power per unit mass,  $\epsilon_{\perp}$  ( $\text{erg g}^{-1} \text{s}^{-1}$ ) from Equation (28), using perpendicular velocity fluctuations from Figure 3. The solid and dashed lines correspond to the range (20-70)  $\text{km s}^{-1}$  (black) from frequency broadening measurements, and (20-40)  $\text{km s}^{-1}$  for  $r < 1.4 R_{\odot}$  for non-thermal velocities from coronal lines (red). **Right:** Coronal heating rate per unit mass ( $\text{erg g}^{-1} \text{s}^{-1}$ ) from Landau damping of ion-sound waves given by Equation (34). As in the right panel of Figure 2, the solid and dashed lines show  $1 \times \overline{q \epsilon^2}$  for  $\alpha = 0.25$  and  $\alpha = 0.4$ , respectively, and the grey area corresponds to the range of values  $[1/2, 2] \times \overline{q \epsilon^2}$ , considering both values of  $\alpha$ .

where  $k_B$  is Boltzmann's constant and  $T_e$  and  $T_i$  are the electron and ion temperatures, respectively. The first term on the right-hand-side of Equation (31) is the electron contribution, while the second term is from protons. For  $T_e \simeq T_i$  ion-sound waves are subject to very strong damping, with a damping rate becoming

$$\gamma_q^s \simeq \sqrt{\frac{\pi}{8e}} v_s q_{\parallel} \simeq 0.4 v_s q_{\parallel} \quad (32)$$

that is a substantial fraction of the wave frequency. This strong damping of the energy associated with ion-sound waves results in a volumetric energy deposition rate ( $\text{erg cm}^{-3} \text{s}^{-1}$ )

$$\frac{dE}{dt} = \int 2\gamma_q^s W_q^s d^3q, \quad (33)$$

or, equivalently, a coronal heating rate per unit mass ( $\text{erg g}^{-1} \text{s}^{-1}$ )

$$\epsilon_i = \frac{1}{\rho} \frac{dE}{dt} = \frac{2}{m_i n} \int \gamma_q^s W_q^s d^3q \simeq 0.8 v_s^3 \int |q_{\parallel}| S(\mathbf{q}) \frac{d^3q}{(2\pi)^3} = 0.8 \alpha v_s^3 \overline{q \epsilon^2}, \quad (34)$$

where the third equality follows from the fact that the ion-sound waves propagate along the (radial) magnetic field. The right panel of Figure 4 shows the heating rate given by Equation (34). The heating profile has a shape that is similar to the heating functions often used in simulations (e.g., Figure 7

in [Cranmer 2010](#)), with a broad maximum at  $(1-3)R_\odot$ , consistent with the observed increasing temperature of the solar corona out to this radius ([Wheatland et al. 1997](#)). The inferred energy deposition rate, integrated over the range of heights  $(2 - 3R_\odot)$  where it is most effective, corresponds to an energy flux,  $\epsilon_i(2R_\odot)m_in(2R_\odot)R_\odot \sim 6 \times 10^5 \text{ erg cm}^{-2} \text{ s}^{-1}$  (600 W) where  $\epsilon_i(2R_\odot) \simeq 10^{11} \text{ erg g}^{-1} \text{ s}^{-1}$  and  $n(2R_\odot) \simeq 5 \times 10^6 \text{ cm}^{-3}$ . We would note that while this value represents a useful constraint on the heating and dynamic energy terms in the corona, directly comparing its magnitude to such terms represents a considerable over-simplification of the modeling of coronal heating and/or solar wind acceleration. Nevertheless, we would point out that such an energy flux is broadly consistent with that required to balance energy losses and so heat the corona (e.g., [Withbroe & Noyes 1977](#); [Hollweg 1986](#); [Withbroe 1988](#)).

The heating rate (34) is proportional to the quantity  $\overline{q\epsilon^2}$ , which, as we have seen, can be inferred from observations related to radio-wave scattering. As shown in Figure 1 of [Kontar et al. \(2023\)](#),  $\overline{q\epsilon^2}$  is dominated by fluctuations at short wavelengths near the inner scale  $q_i^{-1} \sim c/\omega_{pi}$ , so that (their Equation (29)):

$$\overline{q\epsilon^2} \simeq 5 q_i \frac{\langle \delta n_i^2 \rangle}{n^2} . \quad (35)$$

The coronal heating rate per unit mass due to absorption at heliocentric distance  $r$  can therefore be expressed rather succinctly as  $\epsilon_i(r) \simeq 4 \alpha q_i v_s^3 \langle \delta n_i^2 \rangle / n^2$ .

The quantities  $\epsilon_{\ell_\perp}$  and  $\epsilon_i$  are associated with very different physical models, and they are associated with length scales that span five orders of magnitude: the power generated in large-scale Alfvén motions  $\epsilon_{\ell_\perp}$  is dominated by scales  $\ell_\perp(r = 2R_\odot) \simeq 10^4 \text{ km}$ , while the energy dissipation rate  $\epsilon_i$  due to ion-sound wave damping is dominated by waves at the inner scale  $q_i^{-1}$  of the turbulence spectrum, which at  $r = (2 - 3)R_\odot$  is of order 0.1 km. Despite this vast difference in characteristic scales, the quantities  $\epsilon_{\ell_\perp}$  and  $\epsilon_i$  at  $r \simeq (1 - 2)R_\odot$  are very similar; indeed, they are identical within the error bars, with  $\epsilon_{\ell_\perp} \simeq \epsilon_i \simeq 10^{11} \text{ erg g}^{-1} \text{ s}^{-1}$  (Figure 4). This result is both unexpected and tantalizing, suggesting that the energy associated with large-scale magnetic field motions can effectively cascade over the entire inertial range, eventually appearing as small-scale ion-sound waves that are very effectively damped, causing plasma heating. This intriguing result has significant implications for models of coronal heating.

## 8. SUMMARY AND DISCUSSION

Using a density fluctuation model obtained from analysis of solar radio bursts, combined with frequency broadening measurements from various spacecraft, we have deduced the magnitude of the characteristic velocities in the solar corona and the solar wind. The inferred velocities depend on the anisotropy of the density turbulence. The amount of spacecraft signal broadening, and the anisotropic density fluctuation inferred from solar burst data, tell a remarkably coherent story about the level of density turbulence in the solar corona and the bulk flow speeds present; the latter are consistent with previously published values that employed different analysis techniques. The perpendicular velocities are also consistent with the non-thermal speeds deduced from line-of-sight Doppler broadening of spectral lines in the low corona. Interpreted as Alfvén wave amplitudes, these results allow us to determine the amount of energy per unit time transferred in the turbulent cascade from large to small scales, and eventually deposited in the low corona and into the solar wind.

At distances  $r \gtrsim 10R_\odot$ , the frequency broadening is dominated by solar wind motion. The deduced velocity values (200-600)  $\text{km s}^{-1}$  at  $\sim 100 R_\odot$  are consistent with previous scintillation measurements



(e.g., [Ekers & Little 1971](#); [Armstrong & Woo 1981](#)) and are also consistent with characteristic solar wind speeds at these distances (e.g., [Bunting et al. 2024](#)). The anisotropy of density fluctuations appears to be an important ingredient: if the spectrum of density fluctuations were isotropic, only much slower sub-solar-wind speeds (up to  $\sim 100 \text{ km s}^{-1}$ ) would be consistent with the frequency broadening observations; alternatively, the observed frequency broadening would be consistent with observed solar wind speeds only if the level of density fluctuations were much lower than inferred from other observations, such as angular broadening of extra-solar sources.

Closer to the Sun ( $r \lesssim 10 R_{\odot}$ ), however, the solar wind speed becomes small, while the velocities required to explain the frequency broadening observations remain large. The frequency observations require either speeds (20-70)  $\text{km s}^{-1}$  in the perpendicular direction, or (100-300)  $\text{km s}^{-1}$  in the parallel direction or both. Within the description adopted, these two scenarios (or a combination of the two) cannot be meaningfully distinguished.

Given the possible importance of waves and turbulence in the context of solar coronal heating, there are a number of reported results on plasma motions in the corona/solar wind. Plasma motions in the corona between  $(1 - 2) R_{\odot}$  are normally detected using excess (i.e., larger than what would be from thermal motion of the emitting ion) broadening of emission lines from minor ions, and have velocities comparable to those required to realize the observed level of frequency broadening of radio sources. It should be noted that the non-thermal broadening is proportional to the line-of-sight speed (i.e. along the  $\perp_1$  direction), as distinct from the speeds inferred from frequency broadening measurements, which are predominantly along the  $\perp_2$  direction, perpendicular to the line of sight. The similar values of velocity thus suggest azimuthal symmetry in the velocity distribution perpendicular to the radial direction, i.e., to the magnetic field. Similar to the frequency broadening measurements, which are agnostic relative to steady flows versus random “turbulent” velocity patterns with the same root-mean-square speed, there is an ongoing discussion about whether non-thermal broadening of spectral lines is due to bulk plasma flows or to quasi-random ion distribution motions (see discussion in [Jeffrey et al. 2016](#)). Given that ions are preferentially heated via cyclotron resonance ([Seely et al. 1997](#); [Tu et al. 1998](#)), this distinction could be particularly important.

It is interesting to note that there is a broad agreement among the turbulent velocities inferred from interplanetary scintillation measurements (e.g., [Ekers & Little 1971](#); [Armstrong & Woo 1981](#)). Our average values are somewhat smaller, with perpendicular velocities mostly below  $100 \text{ km s}^{-1}$ , with a marginal decrease in speed towards the Sun. Importantly, our results, like those associated with previously reported measurements, show a large spread of values, re-emphasizing a high level of variability of the turbulence level in the solar corona.

Scattering of radio waves requires coherent structures (density fluctuations), which could either be oscillatory in nature or carried by bulk plasma motions. Perpendicular large-scale motions (at scales much larger than the density fluctuation wavelength) could be random torsional or kink (e.g., Alfvén) waves that move around small scale fluctuations. In a turbulent plasma, the spectral broadening may also be associated with large-scale advection of eddies in a Kolmogorov turbulent cascade (e.g., [Tennekes 1975](#)). Quasi-parallel motions or waves parallel to the magnetic field with a speed comparable to the sound (or ion thermal) speed would also produce a similar frequency broadening. [Wexler et al. \(2019\)](#) has interpreted the broadening as due to sound waves. If ion-sound waves are present, one can calculate the energy deposited to ions via Landau damping, and we find a value of or-

der  $10^{11} \text{ erg g}^{-1} \text{ s}^{-1}$ , comparable to the heating required to sustain a million-degree corona (e.g., [Hollweg 1986](#); [Cranmer & van Ballegooijen 2005](#)).

Sound waves do not necessarily propagate from the low atmosphere (although EUV observations suggest propagating slow/sound waves, e.g., [DeForest & Gurman 1998](#)), but could instead be locally generated via parametric decay of Alfvén waves (e.g., [Sagdeev & Galeev 1969](#); [Malara & Velli 1996](#); [Del Zanna et al. 2001](#)) or from MHD turbulence cascade (e.g., [Zank & Matthaeus 1993](#); [Lithwick & Goldreich 2001](#); [Cho & Lazarian 2003](#); [Chandran et al. 2009](#); [Bian et al. 2010](#); [Zank et al. 2017](#)). Since the value of  $\overline{q \epsilon^2}$  depends mostly on the level of density fluctuations near the ion-scale break scale  $q_i^{-1} \sim c/\omega_{pi}$  ([Kontar et al. 2023](#)), the parallel-propagating ion-sound waves Cerenkov resonate mostly with protons and should be strongly Landau damped. This suggests that a constant re-supply of ion-sound waves is required, probably via the aforementioned parametric decay of Alfvén waves and/or the turbulent cascade. Interestingly, the estimate of Kolmogorov cascade power using large scale motions  $v_{\perp}^3/\ell_{\perp}$  (at the outer scales  $\ell_{\perp}$ ) provides the same power that would be dissipated via ion-sound waves at inner scales  $q_i^{-1}$ . Within such a scenario, ion-sound waves (or slow MHD mode waves) act as an intermediate in the coronal heating chain and thus serve as a valuable diagnostic of ion heating in the solar corona.

1 We thank the referee for several very helpful suggestions on how to improve the paper. FA (stu-  
2 dentship 2604774) and EPK were supported via STFC training grant ST/V506692/1. EPK and DLC  
3 were supported via the STFC/UKRI grants ST/T000422/1 and ST/Y001834/1. AGE was supported by  
4 NASA Kentucky under NASA award number 80NSSC21M0362 and by the NASA Heliophysics Support-  
5 ing Research program under award number 80NSSC24K0244. NC acknowledges funding support from  
6 the Initiative Physique des Infinis (IPI), a research training program of the Idex SUPER at Sorbonne  
7 Université.

## APPENDIX

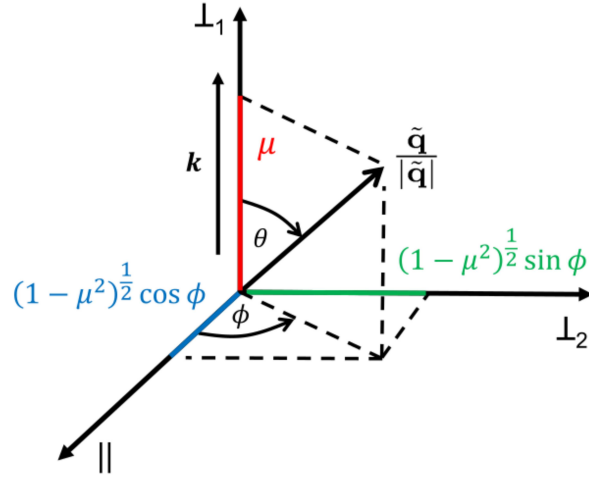
### A. DIFFUSION TENSOR: STATIC DENSITY FLUCTUATIONS

Figure 5 shows the wavevector coordinate system used for our analysis; it is a polar system in the  $\tilde{\mathbf{q}}$  space (in which the density fluctuation spectrum  $S(\tilde{\mathbf{q}})$  is isotropic:  $S(\tilde{\mathbf{q}}) \equiv S(q)$ ). The polar axis is aligned with the  $\perp_1$  direction, which is along the direction of  $\mathbf{k}$  and  $\mathbf{v}_g$  (Figure 5). The direction cosine  $\mu = \cos \theta$ , where  $\theta$  is the polar angle from the  $\perp_1$  axis, while the azimuthal angle  $\phi$  measures the angle from the  $\parallel$  direction in the  $(\tilde{q}_{\parallel}, \tilde{q}_{\perp_2})$  plane. Thus  $\tilde{q}_{\perp_1} = \tilde{q} \mu$ ,  $\tilde{q}_{\perp_2} = \tilde{q} (1 - \mu^2)^{1/2} \sin \phi$  and  $\tilde{q}_{\parallel} = \tilde{q} (1 - \mu^2)^{1/2} \cos \phi$ . Changing variables from  $\mathbf{q} = (q_{\parallel}, q_{\perp_2}, q_{\perp_1})$  to  $\tilde{\mathbf{q}} = \mathbf{A} \mathbf{q} = (\alpha^{-1} q_{\parallel}, q_{\perp_2}, q_{\perp_1})$ , Equation (2) can be written as

$$D_{ij} = \frac{\pi \omega_{pe}^4}{4 \omega^2} \int q_i q_j S(\mathbf{q}) \delta(\mathbf{q} \cdot \mathbf{v}_g) \frac{d^3 q}{(2\pi)^3} = \frac{\pi \omega_{pe}^4}{4 \omega^2} \alpha A_{i\alpha}^{-1} A_{j\beta}^{-1} \int \tilde{q}_{\alpha} \tilde{q}_{\beta} S(\tilde{\mathbf{q}}) \delta(\tilde{\mathbf{q}} \cdot \tilde{\mathbf{v}}_g) \frac{d^3 \tilde{q}}{(2\pi)^3}, \quad (\text{A1})$$

where  $\tilde{\mathbf{v}} = (\alpha v_{\parallel}, v_{\perp_2}, v_{\perp_1})$  and we have used the determinant of the Jacobian  $\det(\mathbf{J}) = \det(\mathbf{A}^{-1}) = \alpha$ .

For elastic scattering and a radio wave propagating along the  $\perp_1$  direction, we can use Equation (A1) to find the various components of the diffusion tensor, viz.



**Figure 5.** Wavevector coordinate system used in our analysis; the radio wave, with wavevector  $\mathbf{k}$ , is propagating along the  $\perp_1$  direction.

$$\begin{aligned}
 D_{\parallel\parallel} &= \frac{\pi \omega_{pe}^4}{4 \omega^2} \alpha^3 \int_{\tilde{q}=0}^{\infty} \int_{\phi=0}^{2\pi} \int_{\mu=-1}^1 \tilde{q}^2 (1 - \mu^2) \cos^2 \phi S(\tilde{q}) \delta(\tilde{q} \tilde{v}_g \mu) \frac{\tilde{q}^2 d\tilde{q} d\mu d\phi}{(2\pi)^3} \\
 &= \frac{\pi \omega_{pe}^4}{4 \omega^2 c} \alpha^3 \int_{\tilde{q}=0}^{\infty} \tilde{q} S(\tilde{q}) \frac{\tilde{q}^2 d\tilde{q}}{(2\pi)^3} = \frac{\pi \omega_{pe}^4}{16 \omega^2 c} \alpha^2 \overline{q \epsilon^2} , \tag{A2}
 \end{aligned}$$

$$\begin{aligned}
 D_{\perp_2 \perp_2} &= \frac{\pi \omega_{pe}^4}{4 \omega^2} \alpha \int_{\tilde{q}=0}^{\infty} \int_{\phi=0}^{2\pi} \int_{\mu=-1}^1 \tilde{q}^2 (1 - \mu^2) \sin^2 \phi S(\tilde{q}) \delta(\tilde{q} \tilde{v}_g \mu) \frac{\tilde{q}^2 d\tilde{q} d\mu d\phi}{(2\pi)^3} \\
 &= \frac{\pi \omega_{pe}^4}{4 \omega^2 c} \alpha \int_{\tilde{q}=0}^{\infty} \int_{\phi=0}^{2\pi} \tilde{q} \sin^2 \phi S(\tilde{q}) \frac{\tilde{q}^2 d\tilde{q} d\phi}{(2\pi)^3} = \frac{\pi \omega_{pe}^4}{16 \omega^2 c} \overline{q \epsilon^2} . \tag{A3}
 \end{aligned}$$

and

$$D_{\perp_1 \perp_1} = \frac{\pi \omega_{pe}^4}{4 \omega^2} \alpha \int_{\tilde{q}=0}^{\infty} \int_{\phi=0}^{2\pi} \int_{\mu=-1}^1 \tilde{q}^2 \mu^2 S(\tilde{q}) \delta(\tilde{q} \tilde{v}_g \mu) \frac{\tilde{q}^2 d\tilde{q} d\mu d\phi}{(2\pi)^3} = 0 . \tag{A4}$$

Further, because  $\int_0^{2\pi} \sin \phi \cos \phi d\phi = 0$  we have  $D_{\perp_2 \parallel} = D_{\parallel \perp_2} = 0$ , while the Dirac delta function in the integral results in  $D_{\perp_1 \parallel} = D_{\parallel \perp_1} = D_{\perp_1 \perp_2} = D_{\perp_2 \perp_1} = 0$ . Thus

$$D = \frac{\pi \omega_{pe}^4}{16 \omega^2 c} \overline{q \epsilon^2} \begin{pmatrix} \alpha^2 & 0 & 0 \\ 0 & 1 & 0 \\ 0 & 0 & 0 \end{pmatrix} \equiv \frac{\pi \omega_{pe}^4}{16 \omega^2 c} \overline{q \epsilon^2} \text{diag}(\alpha^2, 1, 0) , \tag{A5}$$

so that there are only two non-zero elements, neither of which contributes to frequency broadening. These results recover the expressions obtained by [Kontar et al. \(2019\)](#).

## B. DIFFUSION TENSOR: MOVING DENSITY FLUCTUATIONS

B.1. *Parallel Waves*

Consider density fluctuations moving along the  $\parallel$  direction, i.e.,  $\Omega(\mathbf{q}) = v_{\parallel} q_{\parallel}$ . Then from Equation (10), and referring to Figure 5, we find

$$D_{\parallel\parallel} = \frac{\pi\omega_{pe}^4}{4\omega^2} \alpha^3 \int_{\tilde{q}=0}^{\infty} \int_{\phi=0}^{2\pi} \int_{\mu=-1}^1 \tilde{q}^2 (1-\mu^2) \cos^2 \phi S(\tilde{q}) \delta(\tilde{v}_{\parallel} \tilde{q} \sqrt{1-\mu^2} \cos \phi - \tilde{q} \tilde{v}_g \mu) \frac{\tilde{q}^2 d\tilde{q} d\mu d\phi}{(2\pi)^3}, \quad (\text{B6})$$

$$D_{\perp_2\perp_2} = \frac{\pi\omega_{pe}^4}{4\omega^2} \alpha \int_{\tilde{q}=0}^{\infty} \int_{\phi=0}^{2\pi} \int_{\mu=-1}^1 \tilde{q}^2 (1-\mu^2) \sin^2 \phi S(\tilde{q}) \delta(\tilde{v}_{\parallel} \tilde{q} \sqrt{1-\mu^2} \cos \phi - \tilde{q} \tilde{v}_g \mu) \frac{\tilde{q}^2 d\tilde{q} d\mu d\phi}{(2\pi)^3}, \quad (\text{B7})$$

and

$$D_{\perp_1\perp_1} = \frac{\pi\omega_{pe}^4}{4\omega^2} \alpha \int_{\tilde{q}=0}^{\infty} \int_{\phi=0}^{2\pi} \int_{\mu=-1}^1 \tilde{q}^2 \mu^2 S(\tilde{q}) \delta(\tilde{v}_{\parallel} \sqrt{1-\mu^2} \tilde{q} \cos \phi - \tilde{q} \tilde{v}_g \mu) \frac{\tilde{q}^2 d\tilde{q} d\mu d\phi}{(2\pi)^3}. \quad (\text{B8})$$

Noting that  $\tilde{\mathbf{v}} = (\alpha v_{\parallel}, v_{\perp_2}, v_{\perp_1})$ , the delta function can be expanded using the roots of  $g(\mu) = A\sqrt{1-\mu^2} - \mu$ , where  $A = (\tilde{v}_{\parallel}/\tilde{v}_g) \cos \phi \simeq \alpha (v_{\parallel}/c) \cos \phi$ , into

$$\delta(A\sqrt{1-\mu^2} - \mu) = \frac{1}{1+A^2} \delta\left(\mu - \frac{A}{\sqrt{1+A^2}}\right).$$

Thus, integrating over  $\mu$  and retaining up to  $\mathcal{O}(A^2)$  terms, we obtain

$$D_{\parallel\parallel} \simeq \frac{\pi\omega_{pe}^4}{4\omega^2 c} \alpha^3 \int_{\tilde{q}=0}^{\infty} \int_{\phi=0}^{2\pi} \tilde{q} \left(1 - 2 \frac{\tilde{v}_{\parallel}^2}{c^2} \cos^2 \phi\right) \cos^2 \phi S(\tilde{q}) \frac{\tilde{q}^2 d\tilde{q} d\phi}{(2\pi)^3} = \frac{\pi\omega_{pe}^4}{16\omega^2 c} \alpha^2 \left(1 - \frac{3}{2} \alpha^2 \frac{v_{\parallel}^2}{c^2}\right) \overline{q \epsilon^2}, \quad (\text{B9})$$

$$D_{\perp_2\perp_2} = \frac{\pi\omega_{pe}^4}{4\omega^2 c} \alpha \int_{\tilde{q}=0}^{\infty} \int_{\phi=0}^{2\pi} \tilde{q} \left(1 - 2 \frac{\tilde{v}_{\parallel}^2}{c^2} \cos^2 \phi\right) \sin^2 \phi S(\tilde{q}) \frac{\tilde{q}^2 d\tilde{q} d\phi}{(2\pi)^3} = \frac{\pi\omega_{pe}^4}{16\omega^2 c} \left(1 - \frac{1}{2} \alpha^2 \frac{v_{\parallel}^2}{c^2}\right) \overline{q \epsilon^2}, \quad (\text{B10})$$

and

$$D_{\perp_1\perp_1} = \frac{\pi\omega_{pe}^4}{4\omega^2 c} \alpha \int_{\tilde{q}=0}^{\infty} \int_{\phi=0}^{2\pi} \tilde{q} \left(\frac{\tilde{v}_{\parallel}^2}{c^2} \cos^2 \phi\right) S(\tilde{q}) \frac{\tilde{q}^2 d\tilde{q} d\phi}{(2\pi)^3} = \alpha^2 \frac{v_{\parallel}^2}{c^2} \frac{\pi\omega_{pe}^4}{16\omega^2 c} \overline{q \epsilon^2}. \quad (\text{B11})$$

These are modified scattering rate expressions, compared to Equations (A4), (A3) and (A2). However, the corrections are generally small since  $v_{\parallel}^2/c^2 \ll 1$ .

Further, because  $\int_0^{2\pi} \sin \phi d\phi = 0$ ,  $\int_0^{2\pi} \cos \phi d\phi = 0$ , and  $\int_0^{2\pi} \sin \phi \cos \phi d\phi = 0$ , we have, respectively,

$$D_{\perp_1 \perp_2} = D_{\perp_2 \perp_1} = 0; \quad D_{\parallel \perp_1} = D_{\perp_1 \parallel} = 0; \quad D_{\parallel \perp_2} = D_{\perp_2 \parallel} = 0. \quad (\text{B12})$$

Thus the diffusion tensor has the form

$$D = \frac{\pi \omega_{pe}^4}{16 \omega^2 c} \overline{q \epsilon^2} \text{diag} \left( \alpha^2 \left[ 1 - \frac{3}{2} \alpha^2 \frac{v_{\parallel}^2}{c^2} \right], 1 - \frac{1}{2} \alpha^2 \frac{v_{\parallel}^2}{c^2}, \alpha^2 \frac{v_{\parallel}^2}{c^2} \right). \quad (\text{B13})$$

Both  $\parallel$  and  $\perp_2$  directions are perpendicular to the wavevector  $\mathbf{k}$  in this analysis. Hence, for  $\Delta \mathbf{k} \perp \mathbf{k}$  and hence the scattering corresponding to the  $\perp_2 \perp_2$  and  $\parallel \parallel$  terms is elastic. The change to the absolute value of  $|\mathbf{k}|$ , or equivalently the wave frequency  $\omega(\mathbf{k}) \simeq c|\mathbf{k}|$ , comes from the term  $D_{\perp_1 \perp_1} \propto d \langle \Delta k_{\perp_1}^2 \rangle / dt \neq 0$ . Henceforth, we can write

$$D = \frac{\pi \omega_{pe}^4}{16 \omega^2 c} \overline{q \epsilon^2} \text{diag} \left( \alpha^2, 1, \frac{\alpha^2 v_{\parallel}^2}{c^2} \right). \quad (\text{B14})$$

### B.2. Perpendicular Waves

For the case of waves moving in the  $\perp_2$  direction, i.e.,  $\Omega(\mathbf{q}) = v_{\perp_2} q_{\perp_2}$ , the same formalism can be applied here, with  $A = (\tilde{v}_{\perp_2} / \tilde{v}_g) \sin \phi \simeq (v_{\perp_2} / c) \sin \phi$ , to obtain

$$D_{\parallel \parallel} \simeq \frac{\pi \omega_{pe}^4}{4 \omega^2 c} \alpha^3 \int_{\tilde{q}=0}^{\infty} \int_{\phi=0}^{2\pi} \tilde{q} \left( 1 - 2 \frac{\tilde{v}_{\perp_2}^2}{c^2} \sin^2 \phi \right) \cos^2 \phi S(\tilde{q}) \frac{\tilde{q}^2 d\tilde{q} d\phi}{(2\pi)^3} = \frac{\pi \omega_{pe}^4}{16 \omega^2 c} \alpha^2 \left( 1 - \frac{1}{2} \frac{v_{\perp_2}^2}{c^2} \right) \overline{q \epsilon^2}, \quad (\text{B15})$$

$$D_{\perp_2 \perp_2} = \frac{\pi \omega_{pe}^4}{4 \omega^2 c} \alpha \int_{\tilde{q}=0}^{\infty} \int_{\phi=0}^{2\pi} \tilde{q} \left( 1 - 2 \frac{\tilde{v}_{\perp_2}^2}{c^2} \sin^2 \phi \right) \sin^2 \phi S(\tilde{q}) \frac{\tilde{q}^2 d\tilde{q} d\phi}{(2\pi)^3} = \frac{\pi \omega_{pe}^4}{16 \omega^2 c} \left( 1 - \frac{3}{2} \frac{v_{\perp_2}^2}{c^2} \right) \overline{q \epsilon^2}, \quad (\text{B16})$$

and

$$D_{\perp_1 \perp_1} = \frac{\pi \omega_{pe}^4}{4 \omega^2 c} \alpha \int_{\tilde{q}=0}^{\infty} \int_{\phi=0}^{2\pi} \tilde{q} \left( \frac{\tilde{v}_{\perp_2}^2}{c^2} \sin^2 \phi \right) S(\tilde{q}) \frac{\tilde{q}^2 d\tilde{q} d\phi}{(2\pi)^3} = \frac{v_{\perp_2}^2}{c^2} \frac{\pi \omega_{pe}^4}{16 c \omega^2} \overline{q \epsilon^2}. \quad (\text{B17})$$

Again, because  $\int_0^{2\pi} \sin \phi d\phi = 0$ ,  $\int_0^{2\pi} \cos \phi d\phi = 0$ , and  $\int_0^{2\pi} \sin \phi \cos \phi d\phi = 0$ , we have, respectively,

$$D_{\perp_1 \perp_2} = D_{\perp_2 \perp_1} = 0; \quad D_{\parallel \perp_1} = D_{\perp_1 \parallel} = 0; \quad D_{\parallel \perp_2} = D_{\perp_2 \parallel} = 0. \quad (\text{B18})$$

Thus, following the same reasoning as in Equation (B13), the diffusion tensor for perpendicular motions takes the form

$$D = \frac{\pi \omega_{pe}^4}{16 \omega^2 c} \overline{q \epsilon^2} \text{diag} \left( \alpha^2, 1, \frac{v_{\perp_2}^2}{c^2} \right). \quad (\text{B19})$$

### C. DIFFUSION TENSOR: RANDOM MOTIONS

#### C.1. Random Motions Superimposed on a Static Background

Integrating Equation (15) in the approximation  $q_{\perp_2}^2 \langle v_{\perp_2}^2 \rangle \ll q^2 c^2$  and taking  $\Omega = 0$  yields

$$\begin{aligned} D_{\parallel\parallel} &= \frac{\pi \omega_{pe}^4}{4 \omega^2} \alpha^3 \int_{\tilde{q}=0}^{\infty} \int_{\phi=0}^{2\pi} \int_{\mu=-1}^1 \tilde{q}^2 (1 - \mu^2) \cos^2 \phi S(\tilde{q}) \frac{1}{\sqrt{2\pi \tilde{q}_{\perp_2}^2 \langle \tilde{v}_{\perp_2}^2 \rangle}} \exp \left[ -\frac{(\tilde{q} c \mu)^2}{2 \tilde{q}_{\perp_2}^2 \langle \tilde{v}_{\perp_2}^2 \rangle} \right] \frac{d\mu d\phi \tilde{q}^2 d\tilde{q}}{(2\pi)^3} \\ &= \frac{\pi \omega_{pe}^4}{16 \omega^2 c} \alpha^2 \left( 1 - \frac{1}{4} \frac{\langle v_{\perp_2}^2 \rangle}{c^2} \right) \overline{q \epsilon^2} , \end{aligned} \quad (C20)$$

where we have used the substitution  $\xi = \mu c / \sqrt{\langle \tilde{v}_{\perp_2}^2 \rangle}$ , approximated  $q_{\perp_2}^2 \approx q^2 \sin^2 \chi$  and made use of the formula  $\int_{-\infty}^{\infty} \xi^2 \exp(-b \xi^2) d\xi = \sqrt{\pi/4 b^3}$ . In the same way, we find

$$\begin{aligned} D_{\perp_2 \perp_2} &= \frac{\pi \omega_{pe}^4}{4 \omega^2} \alpha \int_{\tilde{q}=0}^{\infty} \int_{\phi=0}^{2\pi} \int_{\mu=-1}^1 \tilde{q}^2 (1 - \mu^2) \sin^2 \phi S(\tilde{q}) \frac{1}{\sqrt{2\pi \tilde{q}_{\perp_2}^2 \langle \tilde{v}_{\perp_2}^2 \rangle}} \exp \left[ -\frac{(\tilde{q} c \mu)^2}{2 \tilde{q}_{\perp_2}^2 \langle \tilde{v}_{\perp_2}^2 \rangle} \right] \frac{d\mu d\phi \tilde{q}^2 d\tilde{q}}{(2\pi)^3} \\ &= \frac{\pi \omega_{pe}^4}{16 \omega^2 c} \alpha \left( 1 - \frac{3}{4} \frac{\langle v_{\perp_2}^2 \rangle}{c^2} \right) \overline{q \epsilon^2} , \end{aligned} \quad (C21)$$

$$\begin{aligned} D_{\perp_1 \perp_1} &= \frac{\pi \omega_{pe}^4}{4 \omega^2} \alpha \int_{\tilde{q}=0}^{\infty} \int_{\phi=0}^{2\pi} \int_{\mu=-1}^1 \tilde{q}^2 \mu^2 S(\tilde{q}) \frac{1}{\sqrt{2\pi \tilde{q}_{\perp_2}^2 \langle \tilde{v}_{\perp_2}^2 \rangle}} \exp \left[ -\frac{(\tilde{q} c \mu)^2}{2 \tilde{q}_{\perp_2}^2 \langle \tilde{v}_{\perp_2}^2 \rangle} \right] \frac{d\mu d\phi \tilde{q}^2 d\tilde{q}}{(2\pi)^3} \\ &= \frac{\langle v_{\perp_2}^2 \rangle}{c^2} \frac{\pi \omega_{pe}^4}{16 \omega^2 c} \overline{q \epsilon^2} , \end{aligned} \quad (C22)$$

and

$$D_{\perp_1 \perp_2} = D_{\perp_2 \perp_1} = 0; \quad D_{\parallel \perp_1} = D_{\perp_1 \parallel} = 0; \quad D_{\parallel \perp_2} = D_{\perp_2 \parallel} = 0 . \quad (C23)$$

The components of the diffusion tensor for random motions (“turbulence”) can then be approximated as

$$D = \frac{\pi \omega_{pe}^4}{16 \omega^2 c} \overline{q \epsilon^2} \text{diag} \left( \alpha^2, 1, \frac{\langle v_{\perp_2}^2 \rangle}{c^2} \right) . \quad (C24)$$

#### C.2. Random Motions Superimposed on Flows in a General Direction

Here we consider random motions superimposed on flows in a general direction perpendicular to  $\mathbf{k}$ . For this purpose we can use the general result

$$\begin{aligned} \int_{\xi=-\infty}^{\infty} B \xi^2 \exp \left( -\frac{B^2}{2} (\xi - A)^2 \right) d\xi &= B \int_{\eta=-\infty}^{\infty} (A + \eta)^2 \exp \left( -\frac{B^2}{2} \eta^2 \right) d\eta = \\ &= B \int_{\eta=-\infty}^{\infty} (A^2 + \eta^2 + 2A\eta) \exp \left( -\frac{B^2}{2} \eta^2 \right) d\eta = \sqrt{2\pi} \left( A^2 + \frac{1}{B^2} \right) \end{aligned} \quad (C25)$$



to compute the components of the diffusion tensor.

We first consider radially propagating density fluctuations, with  $\Omega(\mathbf{q}) = v_{\parallel} q_{\parallel}$ . If we add random motions in the same direction we can evaluate the  $D_{\perp_1 \perp_1}$  term that contributes to the frequency broadening:

$$\begin{aligned} D_{\perp_1 \perp_1} &= \frac{\pi \omega_{pe}^4}{4 \omega^2} \alpha \int_{\tilde{q}=0}^{\infty} \int_{\phi=0}^{2\pi} \int_{\mu=-1}^1 \tilde{q}^2 \mu^2 S(\tilde{q}) \frac{1}{\sqrt{2\pi \tilde{q}_{\parallel}^2 \langle \tilde{v}_{\parallel}^2 \rangle}} \exp \left[ -\frac{(\tilde{q} c \mu - \tilde{q}_{\parallel} \tilde{v}_{\parallel})^2}{2 \tilde{q}_{\parallel}^2 \langle \tilde{v}_{\parallel}^2 \rangle} \right] \frac{d\mu d\phi \tilde{q}^2 d\tilde{q}}{(2\pi)^3} \\ &= \frac{\pi \omega_{pe}^4}{16 \omega^2 c} \frac{1}{q \epsilon^2} \frac{\alpha^2 (v_{\parallel}^2 + \langle v_{\parallel}^2 \rangle)}{c^2}, \end{aligned} \quad (C26)$$

where we have approximated  $\tilde{q}_{\parallel}^2 \approx \tilde{q}^2 \cos^2 \phi$ , made use of the substitution  $\mu = \xi \sqrt{\langle \tilde{v}_{\parallel}^2 \rangle} / c$ , and used Equation (C25).

If we then consider propagation and random motions that are both in the direction perpendicular to the solar radius vector, with dispersion relation  $\Omega(\mathbf{q}) = v_{\perp_2} q_{\perp_2}$ , we find

$$\begin{aligned} D_{\perp_1 \perp_1} &= \frac{\pi \omega_{pe}^4}{4 \omega^2} \alpha \int_{\tilde{q}=0}^{\infty} \int_{\phi=0}^{2\pi} \int_{\mu=-1}^1 \tilde{q}^2 \mu^2 S(\tilde{q}) \frac{1}{\sqrt{2\pi \tilde{q}_{\perp_2}^2 \langle \tilde{v}_{\perp_2}^2 \rangle}} \exp \left[ -\frac{(\tilde{q} c \mu - \tilde{q}_{\perp_2} \tilde{v}_{\perp_2})^2}{2 \tilde{q}_{\perp_2}^2 \langle \tilde{v}_{\perp_2}^2 \rangle} \right] \frac{d\mu d\phi \tilde{q}^2 d\tilde{q}}{(2\pi)^3} \\ &= \frac{\pi \omega_{pe}^4}{16 \omega^2 c} \frac{1}{q \epsilon^2} \frac{v_{\perp_2}^2 + \langle v_{\perp_2}^2 \rangle}{c^2}, \end{aligned} \quad (C27)$$

where we have made use of the substitution  $\mu = \xi \sqrt{\langle \tilde{v}_{\perp_2}^2 \rangle} / c$ , approximated  $\tilde{q}_{\perp_2}^2 \approx \tilde{q}^2 \sin^2 \chi$ , and used Equation (C25).

If both parallel and perpendicular contributions are taken into account, the diffusion tensor takes the form

$$D = \frac{\pi \omega_{pe}^4}{16 \omega^2 c} \frac{1}{q \epsilon^2} \text{diag} \left( \alpha^2, 1, \frac{\alpha^2 (v_{\parallel}^2 + \langle v_{\parallel}^2 \rangle) + v_{\perp_2}^2 + \langle v_{\perp_2}^2 \rangle}{c^2} \right). \quad (C28)$$

Since steady flows  $v^2$  and random motions  $\langle v^2 \rangle$  contribute equally, we can rewrite this as simply

$$D = \frac{\pi \omega_{pe}^4}{16 \omega^2 c} \frac{1}{q \epsilon^2} \text{diag} \left( \alpha^2, 1, \frac{\alpha^2 \langle v_{\parallel}^2 \rangle + \langle v_{\perp_2}^2 \rangle}{c^2} \right), \quad (C29)$$

where now  $\langle \dots \rangle$  includes both steady and random flows, in the parallel or perpendicular directions, respectively, added in quadrature.

#### D. CONVERSION OF REPORTED FREQUENCY BROADENING VALUES TO STANDARD DEVIATIONS

Here we briefly summarize how the frequency broadening in each reported data set, that is not already presented as a standard deviation  $\sigma$ , is converted to give  $\Delta f \equiv \sigma$  for use in Figure 2. We also note

that any reported data that relate to solar transient events have been removed, and we consider only one-way signals.

Goldstein & Stelzried (1967) define the bandwidth as the width of an equivalent rectangle of the same height and area as the measured curves. Comparing with a normalized Gaussian distribution, this implies that the reported bandwidth is  $B = \sqrt{2\pi} \sigma$ , so that  $\Delta f = \sigma = B/\sqrt{2\pi}$ . Yakovlev et al. (1980) define the bandwidth as the “width of the spectral line,” which, absent more detailed specification, we take to be a measure of the standard deviation  $\sigma$ . The signal measurements of Morabito et al. (2003) are provided as  $B = \text{FWHM}$ , which converts as  $\Delta f = \sigma = B/2\sqrt{2 \ln 2}$ . Finally, Woo et al. (1976); Woo (1978); Woo & Armstrong (1979) and Bradford & Routledge (1980) define the bandwidth  $B$  through the relation

$$\int_0^{B/2} P(f) df = \frac{1}{2} \int_0^\infty P(f) df .$$

For a Gaussian distribution with standard deviation  $\sigma$ , this reduces to

$$\text{erf}\left(\frac{B}{2\sqrt{2}\sigma}\right) = \frac{1}{2} ,$$

where the error function is  $\text{erf}(x) = \int_0^x e^{-t^2} dt$ . We thus obtain, for these data sets,

$$\Delta f = \sigma = \left[ 2\sqrt{2} \text{erf}^{-1}\left(\frac{1}{2}\right) \right]^{-1} B \simeq 0.75 B .$$

## E. NON-THERMAL VELOCITIES

The non-thermal velocities are determined from the width  $\zeta$  of the spectrum line profile, measured at the  $1/e$  level, and we retrieve the standard deviation  $v_{\text{nth}} = \zeta/\sqrt{2}$ . We use data from Hassler et al. (1990); Chandrasekhar et al. (1991); Banerjee et al. (1998); Doyle et al. (1998, 1999); Esser et al. (1999); Contesse et al. (2004); Banerjee et al. (2009); Landi & Cranmer (2009); Singh et al. (2011); and Bemporad & Abbo (2012). A summary of the results is presented in Figure 3.

## F. ANALYTICAL APPROXIMATION TO FREQUENCY BROADENING

For the propagation of a radio wave from a distant radio source to the observer at the Earth with a heliocentric angular separation  $r_{\text{obs}} = r(z = 0)$  (see, e.g., Kontar et al. 2023, and Figure 1), there is a frequency broadening given by Equation (21):

$$\frac{\langle \Delta \omega^2 \rangle}{\omega^2} = \frac{\pi}{8 c^2 \omega^4} \int_{\text{los}} \omega_{pe}^4 \left[ \alpha^2 \langle v_{\parallel}^2 \rangle \cos^2 \chi + \langle v_{\perp}^2 \rangle (1 + \sin^2 \chi) \right] \overline{q \epsilon^2} dz . \quad (\text{F30})$$

Assuming that the various quantities in the integral are functions of heliocentric distance  $r = \sqrt{r_{\text{obs}}^2 + z^2}$ , we obtain

$$\begin{aligned} \frac{\langle \Delta \omega^2 \rangle}{\omega^2} = & \frac{2 \pi^3 e^4}{m_e^2 c^2 \omega^4} \int_{-\infty}^{1 \text{ au}} n^2 \left( \sqrt{r_{\text{obs}}^2 + z^2} \right) \overline{q \epsilon^2} \left( \sqrt{r_{\text{obs}}^2 + z^2} \right) \times \\ & \times \left[ \alpha^2 \langle v_{\parallel}^2 \rangle \left( \sqrt{r_{\text{obs}}^2 + z^2} \right) \cos^2 \chi + \langle v_{\perp}^2 \rangle \left( \sqrt{r_{\text{obs}}^2 + z^2} \right) (1 + \sin^2 \chi) \right] dz , \end{aligned} \quad (\text{F31})$$

where we have used  $\omega_{pe} = \sqrt{4\pi ne^2/m_e}$ . With the substitution  $z = r_{\text{obs}} \tan \chi$ , this can be written

$$\begin{aligned} \frac{\langle \Delta \omega^2 \rangle}{\omega^2} &= \frac{2\pi^3 e^4}{m_e^2 c^2 \omega^4} \frac{r_{\text{obs}}}{R_\odot} \int_{-\pi/2}^{\tan^{-1}(215 R_\odot/r_{\text{obs}})} n^2(r_{\text{obs}} \sec \chi) \overline{q \epsilon^2} R_\odot(r_{\text{obs}} \sec \chi) \times \\ &\times \left[ \alpha^2 \langle v_{\parallel}^2 \rangle (r_{\text{obs}} \sec \chi) \cos^2 \chi + \langle v_{\perp}^2 \rangle (r_{\text{obs}} \sec \chi) (1 + \sin^2 \chi) \right] \sec^2 \chi d\chi. \end{aligned} \quad (\text{F32})$$

Figure 6 of [Kontar et al. \(2023\)](#) shows that, empirically,

$$n^2(r_{\text{obs}} \sec \chi) \overline{q \epsilon^2} R_\odot(r_{\text{obs}} \sec \chi) \simeq 6.5 \times 10^{14} \left( \frac{r_{\text{obs}} \sec \chi}{R_\odot} - 1 \right)^{-5.17} \text{ cm}^{-6}. \quad (\text{F33})$$

Using this expression and taking the velocity variances outside the integral as averages, we obtain

$$\begin{aligned} \frac{\langle \Delta \omega^2 \rangle}{\omega^2} &= 6.5 \times 10^{14} \left( \frac{e^4}{8\pi m_e^2 c^2 f^4} \right) \left( \frac{r_{\text{obs}}}{R_\odot} \right)^{-4.17} \times \\ &\times \left\{ \alpha^2 \overline{\langle v_{\parallel}^2 \rangle} \int_{-\pi/2}^{\tan^{-1}(215 R_\odot/r_{\text{obs}})} \left( 1 - \frac{R_\odot \cos \chi}{r_{\text{obs}}} \right)^{-5.17} \cos^{5.17} \chi d\chi + \right. \\ &\left. + \overline{\langle v_{\perp}^2 \rangle} \int_{-\pi/2}^{\tan^{-1}(215 R_\odot/r_{\text{obs}})} \left( 1 - \frac{R_\odot \cos \chi}{r_{\text{obs}}} \right)^{-5.17} \cos^{3.17} \chi (1 + \sin^2 \chi) d\chi \right\}. \end{aligned} \quad (\text{F34})$$

At closest-approach distances  $r_{\text{obs}} \gg R_\odot$ , the term  $(1 - R_\odot \cos \chi / r_{\text{obs}})^{-5.7} \simeq 1$ . Adopting this approximation, the frequency broadening reduces to the relatively simple form

$$\begin{aligned} \frac{\langle \Delta \omega^2 \rangle}{\omega^2} &= 6.5 \times 10^{14} \left( \frac{e^4}{8\pi m_e^2 c^2 f^4} \right) \left( \frac{r_{\text{obs}}}{R_\odot} \right)^{-4.17} \times \\ &\times \left\{ \alpha^2 \overline{\langle v_{\parallel}^2 \rangle} \int_{-\pi/2}^{\chi_{\text{obs}}} \cos^{5.17} \chi d\chi + \overline{\langle v_{\perp}^2 \rangle} \int_{-\pi/2}^{\chi_{\text{obs}}} \cos^{3.17} \chi (1 + \sin^2 \chi) d\chi \right\}. \end{aligned} \quad (\text{F35})$$

where  $\chi_{\text{obs}} = \tan^{-1}(215 R_\odot / r_{\text{obs}})$ . Each integral can be split into two parts: one from  $\chi = -\pi/2$  to 0 (corresponding to the incoming ray from  $\infty$  to the distance of closest approach  $r_{\text{obs}}$ , and other from 0 to  $\chi_{\text{obs}}$ , corresponding to the outgoing ray from  $r_{\text{obs}}$  to 1 au. The integral can then be expressed in terms of beta functions and incomplete beta functions, respectively, viz.

$$\frac{\langle \Delta \omega^2 \rangle^{1/2}}{\omega} = 2.55 \times 10^7 \left( \frac{e^2}{m_e c} \right) \left( \frac{r_{\text{obs}}}{R_\odot} \right)^{-2.085} \left[ \alpha^2 \beta_{\parallel}^2 v_{\parallel, \text{rms}}^2 + \beta_{\perp}^2 v_{\perp, \text{rms}}^2 \right]^{1/2} \times \frac{1}{f^2}, \quad (\text{F36})$$

where we have defined  $v_{\parallel, \text{rms}} = \overline{\langle v_{\parallel}^2 \rangle}^{1/2}$  and  $v_{\perp, \text{rms}} = \overline{\langle v_{\perp}^2 \rangle}^{1/2}$  and

$$\beta_{\parallel} \left( \frac{r_{\text{obs}}}{R_\odot} \right) = \left[ \frac{B(1; 3.085, 0.5) + B(\psi; 3.085, 0.5)}{16\pi} \right]^{1/2}, \quad (\text{F37})$$

$$\beta_{\perp} \left( \frac{r_{\text{obs}}}{R_{\odot}} \right) = \left[ \frac{B(1; 2.085, 0.5) + B(\psi; 2.085, 0.5) + B(1; 2.085, 1.5) + B(\psi; 2.085, 1.5)}{16\pi} \right]^{1/2}. \quad (\text{F38})$$

Here  $B(\psi; u, v)$  are the (incomplete for  $\psi < 1$ ) beta functions corresponding to the integrals  $2 \int_0^{\pi/2} \cos^{5.17} \chi d\chi$ ,  $2 \int_0^{\pi/2} \cos^{3.17} \chi d\chi$ , and  $2 \int_0^{\pi/2} \cos^{3.17} \chi \sin^2 \chi d\chi$ , and  $\psi = \left[ 1 + (r_{\text{obs}}/215R_{\odot})^2 \right]^{-1}$ .

We note that the ratio of the third and first terms in the numerator of the expression for  $\beta_{\perp}$  is

$$\rho_{\perp} = \frac{\Gamma(2.085) \Gamma(1.5) / \Gamma(3.585)}{\Gamma(2.085) \Gamma(0.5) / \Gamma(2.585)} = \frac{0.5}{2.585} \simeq 0.2,$$

so that, given the  $\sqrt{1 + \rho_{\perp}}$  dependence in the expression (F37) for  $\beta_{\perp}$ , the contribution from the  $\sin^2 \chi$  term (which is associated with motions in the  $\perp_1$  direction) to the overall broadening is only about 10%. Moreover, the ratio of the lead terms in the expressions for  $\beta_{\parallel}$  and  $\beta_{\perp}$  is

$$\sqrt{\frac{\Gamma(3.085) \Gamma(0.5) / \Gamma(3.585)}{\Gamma(2.085) \Gamma(0.5) / \Gamma(2.585)}} = \sqrt{\frac{2.085}{2.585}} \simeq 0.9,$$

showing that the contributions from motions in the  $\parallel$  and  $\perp_2$  directions are similar (apart from the anisotropy factor  $\alpha$ ). But, since  $\alpha^2 \ll 1$ , we can, to a good approximation, neglect the contribution from  $v_{\parallel, \text{rms}}$  and write Equation (F36) as

$$\frac{\langle \Delta \omega^2 \rangle^{1/2}}{\omega} = 2.55 \times 10^7 \beta_{\perp} \left( \frac{e^2}{m_e c} \right) \left( \frac{r_{\text{obs}}}{R_{\odot}} \right)^{-2.085} v_{\perp, \text{rms}} \times \frac{1}{f^2}. \quad (\text{F39})$$

Scaling to a nominal frequency of  $f = 1$  GHz (Figure 2), this evaluates to

$$\frac{\Delta f}{f} \simeq 2.1 \times 10^{-13} \beta_{\perp} v_{\perp, \text{rms}} \left( \frac{r_{\text{obs}}}{R_{\odot}} \right)^{-2.085} \left( \frac{1 \text{ GHz}}{f} \right)^2, \quad (\text{F40})$$

where we have written  $\Delta f$  for  $\langle \Delta f^2 \rangle^{1/2}$ . Equation (F40) provides a simple, but nevertheless accurate, analytical approximation for the frequency broadening, valid for  $r_{\text{obs}} \gg R_{\odot}$ . With a nominal  $r_{\text{obs}} = 10 R_{\odot}$ , we obtain  $\beta_{\perp} \simeq 0.25$  and so  $\Delta f/f \simeq 4 \times 10^{-16} v_{\perp, \text{rms}} (f[\text{GHz}])^{-2}$ , corresponding to  $\Delta f \simeq 4 \times 10^{-7} v_{\perp, \text{rms}}$  Hz at  $f = 1$  GHz. Figure 2 shows that  $\Delta f \simeq 3$  Hz at  $r = 10 R_{\odot}$ , corresponding to  $v_{\perp, \text{rms}} \simeq 7.5 \times 10^6$  cm s $^{-1}$ , i.e., 75 km s $^{-1}$ .

## REFERENCES

- |  |   |
|--|---|
| <p>Akhiezer, A. I., Prokhoda, I. G., &amp; Sitenko, A. G. 1958, Soviet Journal of Experimental and Theoretical Physics, 6, 576</p> <p>Anantharamaiah, K. R., Gothoskar, P., &amp; Cornwell, T. J. 1994, Journal of Astrophysics and Astronomy, 15, 387, doi: <a href="https://doi.org/10.1007/BF02714823">10.1007/BF02714823</a></p> | <p>Armstrong, J. W., &amp; Coles, W. A. 1972, J. Geophys. Res., 77, 4602, doi: <a href="https://doi.org/10.1029/JA077i025p04602">10.1029/JA077i025p04602</a></p> <p>Armstrong, J. W., Coles, W. A., Kojima, M., &amp; Rickett, B. J. 1986, in The Sun and the Heliosphere in Three Dimensions, ed. R. G. Marsden &amp; L. A. Fisk, Vol. 123, 59, doi: <a href="https://doi.org/10.1007/978-94-009-4612-5_7">10.1007/978-94-009-4612-5_7</a></p> |
|--|---|

- Armstrong, J. W., Coles, W. A., Kojima, M., & Rickett, B. J. 1990, *ApJ*, 358, 685, doi: [10.1086/169022](https://doi.org/10.1086/169022)
- Armstrong, J. W., & Woo, R. 1981, *A&A*, 103, 415
- Arzner, K., & Magun, A. 1999, *A&A*, 351, 1165
- Banerjee, D., Pérez-Suárez, D., & Doyle, J. G. 2009, *A&A*, 501, L15, doi: [10.1051/0004-6361/200912242](https://doi.org/10.1051/0004-6361/200912242)
- Banerjee, D., Teriaca, L., Doyle, J. G., & Wilhelm, K. 1998, *A&A*, 339, 208
- Bastian, T. S. 1994, *ApJ*, 426, 774, doi: [10.1086/174114](https://doi.org/10.1086/174114)
- Bemporad, A., & Abbo, L. 2012, *ApJ*, 751, 110, doi: [10.1088/0004-637X/751/2/110](https://doi.org/10.1088/0004-637X/751/2/110)
- Bian, N., Emslie, A. G., & Kontar, E. P. 2012, *ApJ*, 754, 103, doi: [10.1088/0004-637X/754/2/103](https://doi.org/10.1088/0004-637X/754/2/103)
- Bian, N. H., Emslie, A. G., & Kontar, E. P. 2019, *ApJ*, 873, 33, doi: [10.3847/1538-4357/ab0411](https://doi.org/10.3847/1538-4357/ab0411)
- Bian, N. H., Kontar, E. P., & Brown, J. C. 2010, *A&A*, 519, A114+, doi: [10.1051/0004-6361/201014048](https://doi.org/10.1051/0004-6361/201014048)
- Bingham, R., Tsytovich, V. N., de Angelis, U., Forlani, A., & Mendonça, J. T. 2003, *Physics of Plasmas*, 10, 3297, doi: [10.1063/1.1588640](https://doi.org/10.1063/1.1588640)
- Bird, M. K. 1982, *SSRv*, 33, 99, doi: [10.1007/BF00213250](https://doi.org/10.1007/BF00213250)
- Blesing, R. G., & Dennison, P. A. 1972, *PASA*, 2, 84, doi: [10.1017/S1323358000012947](https://doi.org/10.1017/S1323358000012947)
- Bradford, H. M., & Routledge, D. 1980, *MNRAS*, 190, 73P, doi: [10.1093/mnras/190.1.73P](https://doi.org/10.1093/mnras/190.1.73P)
- Bunting, K. A., Barnard, L., Owens, M. J., & Morgan, H. 2024, *ApJ*, 961, 64, doi: [10.3847/1538-4357/ad1506](https://doi.org/10.3847/1538-4357/ad1506)
- Celnikier, L. M., Harvey, C. C., Jegou, R., Moricet, P., & Kemp, M. 1983, *A&A*, 126, 293
- Celnikier, L. M., Muschietti, L., & Goldman, M. V. 1987, *A&A*, 181, 138
- Chandran, B. D. G., Quataert, E., Howes, G. G., Xia, Q., & Pongkitiwanchakul, P. 2009, *ApJ*, 707, 1668, doi: [10.1088/0004-637X/707/2/1668](https://doi.org/10.1088/0004-637X/707/2/1668)
- Chandrasekhar, T., Desai, J. N., Ashok, N. M., & Pasachoff, J. M. 1991, *SoPh*, 131, 25, doi: [10.1007/BF00151741](https://doi.org/10.1007/BF00151741)
- Chen, X., Kontar, E. P., Chrysaphi, N., et al. 2020, *ApJ*, 905, 43, doi: [10.3847/1538-4357/abc24e](https://doi.org/10.3847/1538-4357/abc24e)
- Chiba, S., Imamura, T., Tokumaru, M., et al. 2022, *SoPh*, 297, 34, doi: [10.1007/s11207-022-01968-9](https://doi.org/10.1007/s11207-022-01968-9)
- Cho, J., & Lazarian, A. 2003, *MNRAS*, 345, 325, doi: [10.1046/j.1365-8711.2003.06941.x](https://doi.org/10.1046/j.1365-8711.2003.06941.x)
- Chrysaphi, N., Kontar, E. P., Holman, G. D., & Temmer, M. 2018, *ApJ*, 868, 79, doi: [10.3847/1538-4357/aae9e5](https://doi.org/10.3847/1538-4357/aae9e5)
- Chrysaphi, N., Reid, H. A. S., & Kontar, E. P. 2020, *ApJ*, 893, 115, doi: [10.3847/1538-4357/ab80c1](https://doi.org/10.3847/1538-4357/ab80c1)
- Clarkson, D. L., Kontar, E. P., Gordovskyy, M., Chrysaphi, N., & Vilmer, N. 2021, *ApJL*, 917, L32, doi: [10.3847/2041-8213/ac1a7d](https://doi.org/10.3847/2041-8213/ac1a7d)
- Clarkson, D. L., Kontar, E. P., Vilmer, N., et al. 2023, *ApJ*, 946, 33, doi: [10.3847/1538-4357/acbd3f](https://doi.org/10.3847/1538-4357/acbd3f)
- Coles, W. A., & Harmon, J. K. 1989, *ApJ*, 337, 1023, doi: [10.1086/167173](https://doi.org/10.1086/167173)
- Contesse, L., Koutchmy, S., & Viladrich, C. 2004, *Annales Geophysicae*, 22, 3055, doi: [10.5194/angeo-22-3055-2004](https://doi.org/10.5194/angeo-22-3055-2004)
- Cranmer, S. R. 2010, *ApJ*, 710, 676, doi: [10.1088/0004-637X/710/1/676](https://doi.org/10.1088/0004-637X/710/1/676)
- Cranmer, S. R., & van Ballegoijen, A. A. 2005, *ApJS*, 156, 265, doi: [10.1086/426507](https://doi.org/10.1086/426507)
- DeForest, C. E., & Gurman, J. B. 1998, *ApJL*, 501, L217, doi: [10.1086/311460](https://doi.org/10.1086/311460)
- Del Zanna, L., Velli, M., & Londrillo, P. 2001, *A&A*, 367, 705, doi: [10.1051/0004-6361:20000455](https://doi.org/10.1051/0004-6361:20000455)
- Dennison, P. A., & Blesing, R. G. 1972, *Proceedings of the Astronomical Society of Australia*, 2, 86, doi: [10.1017/S1323358000012959](https://doi.org/10.1017/S1323358000012959)
- Dougherty, J. P., & Farley, D. T. 1960, *Proceedings of the Royal Society of London Series A*, 259, 79, doi: [10.1098/rspa.1960.0212](https://doi.org/10.1098/rspa.1960.0212)
- Doyle, J. G., Banerjee, D., & Perez, M. E. 1998, *SoPh*, 181, 91, doi: [10.1023/A:1005019931323](https://doi.org/10.1023/A:1005019931323)
- Doyle, J. G., Teriaca, L., & Banerjee, D. 1999, *A&A*, 349, 956
- Efimov, A. I., Lukanina, L. A., Chashei, I. V., et al. 2020, *Cosmic Research*, 58, 460, doi: [10.1134/S0010952520060040](https://doi.org/10.1134/S0010952520060040)
- Efimov, A. I., Lukanina, L. A., Rudash, V. K., et al. 2013, *Cosmic Research*, 51, 13, doi: [10.1134/S0010952513010036](https://doi.org/10.1134/S0010952513010036)
- Efimov, A. I., Samoznaev, L. N., Andreev, V. E., et al. 2002, *Advances in Space Research*, 30, 453, doi: [10.1016/S0273-1177\(02\)00335-6](https://doi.org/10.1016/S0273-1177(02)00335-6)
- Efimov, A. I., Samoznaev, L. N., Bird, M. K., Chashei, I. V., & Plettemeier, D. 2008, *Advances in Space Research*, 42, 117, doi: [10.1016/j.asr.2008.03.025](https://doi.org/10.1016/j.asr.2008.03.025)
- Ekers, R. D., & Little, L. T. 1971, *A&A*, 10, 310
- Esser, R., Fineschi, S., Dobrzycka, D., et al. 1999, *ApJL*, 510, L63, doi: [10.1086/311786](https://doi.org/10.1086/311786)
- Fokker, A. D. 1965, *BAN*, 18, 111



- Goldman, M. V., & Dubois, D. F. 1982, *Physics of Fluids*, 25, 1062, doi: [10.1063/1.863839](https://doi.org/10.1063/1.863839)
- Goldreich, P., & Sridhar, S. 1995, *ApJ*, 438, 763, doi: [10.1086/175121](https://doi.org/10.1086/175121)
- Goldstein, M. L., Roberts, D. A., & Matthaeus, W. H. 1995, *ARA&A*, 33, 283, doi: [10.1146/annurev.aa.33.090195.001435](https://doi.org/10.1146/annurev.aa.33.090195.001435)
- Goldstein, R. M., & Stelzried, C. 1967, *The superior conjunction of Mariner IV (Jet Propulsion Laboratory, California Institute of Technology)*
- Gordovskyy, M., Kontar, E., Browning, P., & Kuznetsov, A. 2019, *ApJ*, 873, 48, doi: [10.3847/1538-4357/ab03d8](https://doi.org/10.3847/1538-4357/ab03d8)
- Gupta, G. R., Teriaca, L., Marsch, E., Solanki, S. K., & Banerjee, D. 2012, *A&A*, 546, A93, doi: [10.1051/0004-6361/201219795](https://doi.org/10.1051/0004-6361/201219795)
- Hassler, D. M., Rottman, G. J., Shoub, E. C., & Holzer, T. E. 1990, *ApJL*, 348, L77, doi: [10.1086/185635](https://doi.org/10.1086/185635)
- Hewish, A. 1958, *MNRAS*, 118, 534, doi: [10.1093/mnras/118.6.534](https://doi.org/10.1093/mnras/118.6.534)
- Hollweg, J. V. 1978, *Reviews of Geophysics and Space Physics*, 16, 689, doi: [10.1029/RG016i004p00689](https://doi.org/10.1029/RG016i004p00689)
- . 1986, *J. Geophys. Res.*, 91, 4111, doi: [10.1029/JA091iA04p04111](https://doi.org/10.1029/JA091iA04p04111)
- Ingale, M., Subramanian, P., & Cairns, I. 2015, *MNRAS*, 447, 3486, doi: [10.1093/mnras/stu2703](https://doi.org/10.1093/mnras/stu2703)
- Jeffrey, N. L. S., Fletcher, L., & Labrosse, N. 2016, *A&A*, 590, A99, doi: [10.1051/0004-6361/201527986](https://doi.org/10.1051/0004-6361/201527986)
- Jeffrey, N. L. S., Kontar, E. P., Bian, N. H., & Emslie, A. G. 2014, *ApJ*, 787, 86, doi: [10.1088/0004-637X/787/1/86](https://doi.org/10.1088/0004-637X/787/1/86)
- Kellogg, P. J. 2020, *ApJ*, 891, 51, doi: [10.3847/1538-4357/ab7003](https://doi.org/10.3847/1538-4357/ab7003)
- Kontar, E. P., Emslie, A. G., Clarkson, D. L., et al. 2023, *ApJ*, 956, 112, doi: [10.3847/1538-4357/acf6c1](https://doi.org/10.3847/1538-4357/acf6c1)
- Kontar, E. P., Perez, J. E., Harra, L. K., et al. 2017a, *PhRvL*, 118, 155101, doi: [10.1103/PhysRevLett.118.155101](https://doi.org/10.1103/PhysRevLett.118.155101)
- Kontar, E. P., Yu, S., Kuznetsov, A. A., et al. 2017b, *Nature Communications*, 8, 1515, doi: [10.1038/s41467-017-01307-8](https://doi.org/10.1038/s41467-017-01307-8)
- Kontar, E. P., Chen, X., Chrysaphi, N., et al. 2019, *ApJ*, 884, 122, doi: [10.3847/1538-4357/ab40bb](https://doi.org/10.3847/1538-4357/ab40bb)
- Krall, N. A., & Trivelpiece, A. W. 1973, *Principles of plasma physics* (Tokyo: McGraw-Hill)
- Krupar, V., Maksimovic, M., Kontar, E. P., et al. 2018, *ApJ*, 857, 82, doi: [10.3847/1538-4357/aab60f](https://doi.org/10.3847/1538-4357/aab60f)
- Krupar, V., Szabo, A., Maksimovic, M., et al. 2020, *ApJS*, 246, 57, doi: [10.3847/1538-4365/ab65bd](https://doi.org/10.3847/1538-4365/ab65bd)
- Kuznetsov, A. A., Chrysaphi, N., Kontar, E. P., & Motorina, G. 2020, *ApJ*, 898, 94, doi: [10.3847/1538-4357/aba04a](https://doi.org/10.3847/1538-4357/aba04a)
- Landi, E., & Cranmer, S. R. 2009, *ApJ*, 691, 794, doi: [10.1088/0004-637X/691/1/794](https://doi.org/10.1088/0004-637X/691/1/794)
- Leer, E., Holzer, T. E., & Fla, T. 1982, *SSRv*, 33, 161, doi: [10.1007/BF00213253](https://doi.org/10.1007/BF00213253)
- Lithwick, Y., & Goldreich, P. 2001, *ApJ*, 562, 279, doi: [10.1086/323470](https://doi.org/10.1086/323470)
- Lyubchik, O., Kontar, E. P., Voitenko, Y. M., Bian, N. H., & Melrose, D. B. 2017, *SoPh*, 292, 117, doi: [10.1007/s11207-017-1140-1](https://doi.org/10.1007/s11207-017-1140-1)
- Machin, K. E., & Smith, F. G. 1952, *Nature*, 170, 319, doi: [10.1038/170319b0](https://doi.org/10.1038/170319b0)
- Maguire, C. A., Carley, E. P., Zucca, P., Vilmer, N., & Gallagher, P. T. 2021, *ApJ*, 909, 2, doi: [10.3847/1538-4357/abda51](https://doi.org/10.3847/1538-4357/abda51)
- Malara, F., & Velli, M. 1996, *Physics of Plasmas*, 3, 4427, doi: [10.1063/1.872043](https://doi.org/10.1063/1.872043)
- Marsch, E., & Tu, C. Y. 1990, *J. Geophys. Res.*, 95, 11945, doi: [10.1029/JA095iA08p11945](https://doi.org/10.1029/JA095iA08p11945)
- McCauley, P. I., Cairns, I. H., & Morgan, J. 2018, *SoPh*, 293, 132, doi: [10.1007/s11207-018-1353-y](https://doi.org/10.1007/s11207-018-1353-y)
- Mejia-Ambriz, J. C., Jackson, B. V., Gonzalez-Esparza, J. A., et al. 2015, *SoPh*, 290, 2539, doi: [10.1007/s11207-015-0694-z](https://doi.org/10.1007/s11207-015-0694-z)
- Mohan, A. 2021, *A&A*, 655, A77, doi: [10.1051/0004-6361/202142029](https://doi.org/10.1051/0004-6361/202142029)
- Morabito, D. D. 2009, *Radio Science*, 44, RS6004, doi: [10.1029/2008RS004002](https://doi.org/10.1029/2008RS004002)
- Morabito, D. D., Shambayati, S., Finley, S., & Fort, D. 2003, *IEEE Transactions on Antennas and Propagation*, 51, 201, doi: [10.1109/TAP.2003.809055](https://doi.org/10.1109/TAP.2003.809055)
- Murphy, P. C., Carley, E. P., Ryan, A. M., Zucca, P., & Gallagher, P. T. 2021, *A&A*, 645, A11, doi: [10.1051/0004-6361/202038518](https://doi.org/10.1051/0004-6361/202038518)
- Musset, S., Maksimovic, M., Kontar, E., et al. 2021, *A&A*, 656, A34, doi: [10.1051/0004-6361/202140998](https://doi.org/10.1051/0004-6361/202140998)
- Parker, E. N. 1958, *ApJ*, 128, 664, doi: [10.1086/146579](https://doi.org/10.1086/146579)
- Pécseli, H. 2012, *Waves and Oscillations in Plasmas* (Boca Raton: CRC Press), doi: [10.1201/b12702](https://doi.org/10.1201/b12702)
- Ratcliffe, H., Bian, N. H., & Kontar, E. P. 2012, *ApJ*, 761, 176, doi: [10.1088/0004-637X/761/2/176](https://doi.org/10.1088/0004-637X/761/2/176)



- Razmanov, V. M., Efimov, A. I., & Yakoviev, O. I. 1980, *Radiophysics and Quantum Electronics*, 22, 728, doi: [10.1007/BF01035278](https://doi.org/10.1007/BF01035278)
- Riddle, A. C. 1974, *SoPh*, 35, 153, doi: [10.1007/BF00156964](https://doi.org/10.1007/BF00156964)
- Sagdeev, R. Z., & Galeev, A. A. 1969, *Nonlinear Plasma Theory* (New York: Benjamin)
- Seely, J. F., Feldman, U., Schühle, U., et al. 1997, *ApJL*, 484, L87, doi: [10.1086/310769](https://doi.org/10.1086/310769)
- Sharma, R., & Oberoi, D. 2021, *ApJ*, 913, 153, doi: [10.3847/1538-4357/ac01df](https://doi.org/10.3847/1538-4357/ac01df)
- Singh, J., Hasan, S. S., Gupta, G. R., Nagaraju, K., & Banerjee, D. 2011, *SoPh*, 270, 213, doi: [10.1007/s11207-011-9732-7](https://doi.org/10.1007/s11207-011-9732-7)
- Steinberg, J. L. 1972, *A&A*, 18, 382
- Stores, M., Jeffrey, N. L. S., & Kontar, E. P. 2021, *ApJ*, 923, 40, doi: [10.3847/1538-4357/ac2c65](https://doi.org/10.3847/1538-4357/ac2c65)
- Stverak, S., Trávníček, P. M., & Hellinger, P. 2015, *Journal of Geophysical Research (Space Physics)*, 120, 8177, doi: [10.1002/2015JA021368](https://doi.org/10.1002/2015JA021368)
- Tennekes, H. 1975, *Journal of Fluid Mechanics*, 67, 561, doi: [10.1017/S00222112075000468](https://doi.org/10.1017/S00222112075000468)
- Thejappa, G., & MacDowall, R. J. 2008, *ApJ*, 676, 1338, doi: [10.1086/528835](https://doi.org/10.1086/528835)
- Tsyтович, V. N., & ter Haar, D. 1995, *Lectures on Non-linear Plasma Kinetics* (Springer-Verlag, Berlin, Heidelberg, New York)
- Tu, C. Y., & Marsch, E. 1995, *SSRv*, 73, 1, doi: [10.1007/BF00748891](https://doi.org/10.1007/BF00748891)
- Tu, C. Y., Marsch, E., Wilhelm, K., & Curdt, W. 1998, *ApJ*, 503, 475, doi: [10.1086/305982](https://doi.org/10.1086/305982)
- Wang, J., Chhiber, R., Roy, S., et al. 2024, *arXiv e-prints*, arXiv:2402.05191, doi: [10.48550/arXiv.2402.05191](https://doi.org/10.48550/arXiv.2402.05191)
- Wang, T. J., Ofman, L., & Davila, J. M. 2009, *ApJ*, 696, 1448, doi: [10.1088/0004-637X/696/2/1448](https://doi.org/10.1088/0004-637X/696/2/1448)
- West, M. J., Seaton, D. B., Wexler, D. B., et al. 2023, *SoPh*, 298, 78, doi: [10.1007/s11207-023-02170-1](https://doi.org/10.1007/s11207-023-02170-1)
- Wexler, D., Imamura, T., Efimov, A., et al. 2020, *SoPh*, 295, 111, doi: [10.1007/s11207-020-01677-1](https://doi.org/10.1007/s11207-020-01677-1)
- Wexler, D. B., Hollweg, J. V., Efimov, A. I., et al. 2019, *ApJ*, 871, 202, doi: [10.3847/1538-4357/aaf6a8](https://doi.org/10.3847/1538-4357/aaf6a8)
- Wheatland, M. S., Sturrock, P. A., & Acton, L. W. 1997, *ApJ*, 482, 510, doi: [10.1086/304133](https://doi.org/10.1086/304133)
- Wilczek, M., & Narita, Y. 2012, *PhRvE*, 86, 066308, doi: [10.1103/PhysRevE.86.066308](https://doi.org/10.1103/PhysRevE.86.066308)
- Withbroe, G. L. 1988, *ApJ*, 325, 442, doi: [10.1086/166015](https://doi.org/10.1086/166015)
- Withbroe, G. L., & Noyes, R. W. 1977, *ARA&A*, 15, 363, doi: [10.1146/annurev.aa.15.090177.002051](https://doi.org/10.1146/annurev.aa.15.090177.002051)
- Woo, R. 1978, *ApJ*, 219, 727, doi: [10.1086/155831](https://doi.org/10.1086/155831)
- . 1996, *Ap&SS*, 243, 97, doi: [10.1007/BF00644038](https://doi.org/10.1007/BF00644038)
- Woo, R., & Armstrong, J. W. 1979, *J. Geophys. Res.*, 84, 7288, doi: [10.1029/JA084iA12p07288](https://doi.org/10.1029/JA084iA12p07288)
- Woo, R., & Gazis, P. 1993, *Nature*, 366, 543, doi: [10.1038/366543a0](https://doi.org/10.1038/366543a0)
- Woo, R., & Goldstein, R. M. 1994, *Geophys. Res. Lett.*, 21, 85, doi: [10.1029/93GL03389](https://doi.org/10.1029/93GL03389)
- Woo, R., Yang, F. C., & Ishimaru, A. 1976, *ApJ*, 210, 593, doi: [10.1086/154864](https://doi.org/10.1086/154864)
- Yakovlev, O. I., Efimov, A. I., Razmanov, V. M., & Shtrykov, V. K. 1980, *Soviet Ast.*, 24, 454
- Yakovlev, O. I., & Pisanko, Y. V. 2018, *Advances in Space Research*, 61, 552, doi: [10.1016/j.asr.2017.10.052](https://doi.org/10.1016/j.asr.2017.10.052)
- Zank, G. P., Adhikari, L., Hunana, P., et al. 2017, *ApJ*, 835, 147, doi: [10.3847/1538-4357/835/2/147](https://doi.org/10.3847/1538-4357/835/2/147)
- Zank, G. P., & Matthaeus, W. H. 1993, *Physics of Fluids A*, 5, 257, doi: [10.1063/1.858780](https://doi.org/10.1063/1.858780)
- Zank, G. P., Zhao, L., Adhikari, L., et al. 2024, *arXiv e-prints*, arXiv:2403.14861, doi: [10.48550/arXiv.2403.14861](https://doi.org/10.48550/arXiv.2403.14861)